

Solute transport and water flow in an unsaturated, heterogeneous profile with root water uptake

MSc Thesis

Jip de Vries

911218914060

SLM-80336

Soil Physics and Land Management, Wageningen University

Supervisors: Sjoerd van der Zee and Toon Leijnse

January 2016



Summary

Pollutant leaching in heterogeneous soil towards groundwater is modelled for both steady state and transient flow. Next to that, the importance of including root water uptake in a transport model with a degrading solute is considered. Simulations are performed in Hydrus-2D. Heterogeneity is mimicked using an auto-correlated random field using the scaling parameter to produce a stochastic field for hydraulic conductivity and water content. Using several scenarios with differences in inflow, timing of solute application and root water uptake, we study flow and solute transport.

Preferential flow paths, resulting from the heterogeneity in conductivity, are quantified using variograms of the output fields. The results show that the initial conditions before solute application influence the transport: low inflow initial conditions before a solute application with high inflow (e.g. during a rain event) cause the solute to move down slightly slower than it would have in a situation in which it would have rained just before the application. In a case with multiple solute applications with varying inflow, a solute applied with high inflow can overtake an earlier front that has been applied with low inflow. The first front is then compressed, i.e. the variance around the centre of mass decreases. After the second front has caught up with the first front, both solutes move further in the high-input flow paths. It is also found that the solute-front lags behind the soil moisture-front when high flow is following low flow.

It appears to be important for predicting solute leaching, that root water uptake is accounted for explicitly. Assumed is that below the root zone, infiltration is the same in cases with and without root water uptake. Due to higher velocities in the root zone when root water uptake is considered compared to a case where the net percolation is taken, the breakthrough curve sets in earlier, has a higher peak and is tailed towards the larger travel times. These effects become stronger when the effective infiltration decreases. For the considered parametrisation, the narrow capillary fringe did not affect water saturation in the root zone and therefore neither affected solute breakthrough for a plane directly below the root zone. Also, for the considered parametrisation, even when saturation and precipitation conditions result in a shift in hydraulic structure, the influence on the breakthrough is limited. These results can be used to develop a method to include the realistic effects of root water uptake in a simpler model without having to consider the detailed processes.

All these spatial patterns in solute spreading become important when the leaching of a chemical to the groundwater is considered. Concentrated chemicals could degrade slower because of limiting conditions (electron acceptors, microbial mass), or an overtaking front could enhance leaching to the groundwater. Regarding the solutes on the one hand and enhancing leaching on the other, these results show that transient conditions and root water uptake should be considered to predict pesticide leaching to the groundwater.

Table of Contents

1. Introduction	1
1.1. Problem and Relevance	1
1.2. Research objectives	1
1.3. Hypotheses	2
1.3.1. Preferential flow	2
1.3.2. Root water uptake	3
2. Literature Review	4
2.1. De-icing chemicals	4
2.2. Water flow and solute transport	5
2.3. Root water uptake	7
3. Methodology	9
3.1. Model structure	9
3.1.1. Basic model	9
3.1.2. Root water uptake module	10
3.2. Scenarios	11
3.2.1. Preferential flow scenarios	11
3.2.2. Root water uptake scenarios	11
3.3. Analysis	12
4. Results and Discussion	15
4.1. Quantification of preferential flow paths	15
4.2. Influence of initial conditions on flow pattern	19
4.3. Solute spreading behaviour under transient water flow	20
4.4. Differences in movement of solute- and waterfront	23
4.5. Precipitation-evaporation series including root water uptake	25
4.6. Solute spreading with critical regime shift at the root zone	27
4.7. Influence of the groundwater table depth and root water uptake on solute leaching	28
4.8. Effect of including root water uptake in a model on solute leaching	29
5. Conclusion	31
6. Acknowledgements	33
Appendices	i
A. Model runs	i
B. Figures	iii

1. Introduction

1.1. Problem and Relevance

The Gardermoen airport in Oslo is built over a large aquifer, which is used for drinking water extraction. The quality of this groundwater has to be safeguarded because of seepage into streams and other withdrawals for use in households.

At Oslo airport, 1000-2000 tons of propylene glycol (PG) and 200 tons of potassium formate (KFo) are used per winter season, of which a significant amount ends up near runways by snow clearing and blast [40]. Normally, these chemicals are biodegradable, but because the leaching mainly occurs during snow melt a seasonal overload can take place. Also, the low temperatures during winter are not favourable for degradation. Then, the microorganisms in the soil, which are functioning as a filter, cannot break down the chemicals quickly enough before they are leached into the groundwater.

Therefore there is a risk that used de-icing chemicals leach out to the groundwater, but the extent of this leakage is not well known yet. This knowledge gap gave rise to research on how de-icing chemicals spread in the unsaturated zone, on how they are degraded, on how degradation can be enhanced and on the likelihood these substances will reach the groundwater before being broken down in the soil.

When broken down in the presence of oxygen, these substances will cause no problems. However, when these chemicals are broken down anaerobically, unwanted substances such as mercaptanes and methanes can be produced. The former has a bad odour and is toxic and the latter is explosive, which is highly unwanted below an airport [27, 35, 40]. Because of the slow diffusion of oxygen from the atmosphere into the soil, this slower anaerobic degradation also takes place deeper in the unsaturated zone. For this reason, for the chemicals which have ended up in the soil and groundwater, remedial actions are needed.

Therefore it is important to know how solutes are spreading in a heterogeneous soil, under different conditions (i.e. atmospheric boundary conditions, timing of solute application and presence of root water uptake), and what processes influence the leaching to the groundwater.

Similar processes and risks are encountered in other cases as well: airports located in colder environments with similar hydrogeological conditions (Germany, Scandinavia and North America) using de-icing chemicals for runways and airplanes are also dealing with leaching of these components to groundwater [12].

1.2. Research objectives

For predicting how solutes behave in the subsurface, it is especially important to know about the transport processes in the unsaturated zone. This is because the travel time of the solute in this zone is an important factor controlling leakage, determining the time available for degradation. Many studies on predicting solute spreading include a set of realistic boundary conditions, among which transient inflow, heterogeneous media, multiple dimensions, solutions interacting with the matrix and more. However, in this context it has not been simulated yet how preferential flow processes in a medium with heterogeneous conductivity explain the spreading behaviour of a solute during transient inflow.

Root water uptake is a process which is usually included in simulations in a simplified manner. However, this process is depending on the pressure heads in the soil, and therefore the water will be taken up heterogeneously. This becomes interesting when the spatial and temporal spreading of solutes is studied, and therefore the influence of root water uptake will be considered here.

The aim of this study is therefore to find how contaminants are spreading in the unsaturated zone during transient flow in a heterogeneous medium, including root water uptake. By using a numerical model to make simulations for different simplified scenarios, it will be possible to deduce how a solute behaves for the given boundary conditions.

Mixing of different types of water in case of a variable flux will be studied, where the components characterising the type of water are not reactive. Also, the spreading of a degrading chemical in the presence of root water uptake will be studied. In this way, the spreading mechanism of the solutes can be found.

When the processes found here will be taken into account when considering leakage, a more realistic view on what happens in the unsaturated zone will be obtained and more realistic estimates on risk of leakage can be made.

The first step is partly accomplished by A. Dathe:

1. To develop a model which simulates non-reactive particle transport for transient water flow in an unsaturated heterogeneous medium,

The objectives for this study building further on this first step are:

2. Use the previously developed model to investigate how changing infiltration influences the leaching of solutes,

With the related research questions:

- a) How can the preferential flow paths be quantified (correlation length of parameter fields, size of flow fingers)?
- b) How do initial conditions of the flow domain influence the flow pattern?
- c) How do the different types of water relate in velocity?
- d) How do the positions of solute- and water fronts relate?

3. Develop the model further to find the effect of including root water uptake in an unsaturated zone simulation on solute transport.

With the research questions:

- a) What is the difference in leached mass (total, spatial and temporal distribution) in a case with and without root water uptake?
- b) When does the root zone dominate in the effect on pesticide transport? How are the subsoil depth and net percolation influencing breakthrough?

1.3. Hypotheses

1.3.1. Preferential flow

The hypotheses will be tested by doing simulations as shown in Appendix A. These will clarify how particles are spreading by highlighting a specific process taking place. From the first steady-state simulations the preferential flow paths can be quantified. Further down this is explained in more detail. In the steady state simulations, we expect to see here a shift in hydraulic structure, as modelled before by [22].

When the steady-state simulation with a solute is compared to the simulation where the solute is added after the shift in flow regime, we will be able to see the influence of the initial

conditions on the solute spreading. The previous flow regime, let it be high or low, will have caused the water content and pressure heads to change. With higher initial soil moisture, a better connectivity is expected, which results in quicker transport than in a case with low initial soil moisture content.

From the transient simulations with two solutes we may see how the two different 'types' of water relate concerning their velocity. For example, when in the first scenario the inflow at the top shifts from high to low, or vice versa, the preferential flow paths can be expected to shift sideways. From the model, we will be able to see if the solute is taken with the flow and spreads sideways as well. It could also be that the two types of water take different routes. When the actual contaminant fluid is in this last pulse, it will move down quickly and could be bypassing the first solute pulse which is located now in the low-conductivity flow paths. In that case the water types would not mix. For the relation between solute- and water front we might see that these have a different velocity due to different spaces to fill up with water resp. solute.

1.3.2. Root water uptake

In case of root water uptake (RWU), the net percolation at the bottom of the root zone should be the same as in a case without RWU. A difference would be the route of the water. In a case without RWU, the evaporation would already be subtracted and the net amount of water infiltrates. In a case with RWU, a larger volume infiltrates, of which a part is taken up by the roots, particularly at certain high-pressure locations. This implies that the flow of water is decreased or rerouted. However, the saturation is higher at the top of the domain so there the soil has a higher conductivity, consequently increasing the infiltration velocity.

A larger spread in the breakthrough curve over time is expected for a case with RWU compared to a situation without. This, because on the one hand, higher inflow will result in faster flow routes and an earlier arrival of the solute. On the other hand, rerouting of the water because of root water uptake, including the transported solute, could decrease water flow in some areas and result in larger travel times.

In these simulations also degradation will be taken into account. This will be visible in the smaller total concentrations of the breakthrough curve. Differences in travel times will imply different total concentrations leaching out.

By running scenarios for different climatic conditions, we can deduce the influence of the upper root zone layer. This will also be tested by running a set of scenarios with shallower groundwater tables. In case of a larger net percolation amount, the front will move quicker and the breakthrough will be timed earlier. Differences in the form of the breakthrough curve (BTC) could occur as well: start time of breakthrough, time of maximum breakthrough, symmetry, and total surface. Even when the exact processes behind the root water uptake influence on leaching are not known, including the RWU in a model would still be better than leaving it out, as it makes predictions more realistic.

In the following Chapter, an overview of relevant background literature will be given, for de-icing chemicals in general, for preferential flow processes and for root water uptake. The methods will be explained in Chapter 3. This includes the setup of the conceptual model, the chosen scenarios to simulate relevant situations and the statistical analysis carried out. This is followed by Chapter 4 where results and discussion is given per research question. First the subjects related to solute transport under the influence of changing infiltration are described, later the subjects related to root water uptake. Conclusions are listed in Chapter 5.

2. Literature Review

2.1. De-icing chemicals

The role of de-icing chemicals in the environment has been subject to extensive research already [2, 12, 15, 40, 31]. In these studies, the focus was predominantly on the microbial degradation as well as the plume development (i.e. spreading behaviour) of the chemicals in the soil and the evaluation of remediation techniques.

De-icing chemicals usually decrease the melting point of water. Different chemicals are used for aircraft and runways. The aircraft de-icing chemical considered here is the small organic molecule propylene glycol (PG). This substance is degradable under both aerobic and anaerobic conditions. The aerobic degradation pathway involves steps through several organic acids, to the final formation of water and carbon dioxide. When de-icing chemicals end up on the soil, several physical and chemical processes govern its spread and transport further downstream. These are flow processes (infiltration, drainage, redistribution and capillary upward flow), solute transport processes (advection, diffusion, dispersion), and biogeochemical interactions (degradation). These processes vary in space and time, which makes transport of these chemicals hard to predict.

The main infiltration of the solutes takes place during spring, when the snow that has been removed from the runways and accumulated close by is melting. Due to differences in the surface topography, the infiltration is not homogeneously distributed over the area. French et al. (1999) found that the main mechanisms determining the spreading of infiltrating water at a test plot near the airport are surface microtopography, snow melt variations and the heterogeneity of the soil itself. Of these, the spatiotemporal variability in physical properties of the soil was found to be the dominating factor, therefore, such variability should be emphasised in the prediction of solute transport [10, 29]. Concerning the temporal variability, there is a distinct seasonality in the infiltration pattern in that part of Norway: The precipitation that has accumulated during winter will infiltrate and carry the chemicals with it, until the moment that evaporation balances precipitation. Then the infiltration front halts. The movement continues during the autumn rains [10].

As soon as the de-icing fluids are located in the soil, degradation by microorganisms commences. Microbial activity is predominantly found in the top layer of the soil and decreases profoundly in the downward direction [2]. However, these degradation mechanisms are less effective than they could be. Because of the high chemical oxygen demand of PG degradation in combination with impeded oxygen transport downwards in soil, the subsoil may become oxygen-depleted. Other constituents in the soil may then act as electron acceptors in the microbial mineralisation of PG, e.g. nitrate, manganese and iron oxides. Usually, PG degradation is a slower process under those conditions.

French et al. [9] studied transport and degradation of PG in the unsaturated zone and found that de-icing chemicals will bypass the potentially most active degradation zone. The results of Schotanus (2013) support this [28]. At a 1 m depth, the effect of the water flow (the thickness of the snow cover) dominates over the effect of the degradation parameters on the leaching, because with a large amount of input (i.e. melt water) and a low temperature, there is less time and potential for degradation [28]. In other words, degradation of PG is strongly controlled by the low temperatures and travel times in the upper soil [15].

From these studies, it follows that remediation techniques could focus on increasing residence time and microbial activity to enhance degradation.

2.2. Water flow and solute transport

In addition to the degradation, a set of physical properties of the soil determine how the de-icing fluid is transported. In general, transport in the unsaturated zone is a function of the medium properties and the driving forces: hydraulic conductivity, soil moisture, matric and gravitational potential. The complicating factor is the fact that the area consists of a very heterogeneous soil: glaciofluvial sand deposits. Variations in the grain size correspond with water retention properties and therefore with variations in water content and hydraulic conductivity.

In the unsaturated zone, especially at high saturation, a large part of the flow may occur in a small fraction of the medium. This preferential flow is an uneven and quick movement of the water, opposed to matrix flow, which occurs relatively slow and evenly. Preferential flow occurs in three types: as a result of macropore flow, as finger flow or unstable flow at the surface, or in regions with textural interfaces in the medium, deflecting the flow (funnel flow) [18]. A typical characteristic of preferential flow is that during wetting, part of the moisture front can propagate quickly to significant depths while bypassing a large part of the matrix pore-space [43]. Thereby, preferential flow affects the leaching of chemicals. Not only the higher flow rates increase the leaching, but also the fact that the transported contaminants are in contact with a smaller part of the medium, which reduces the possibility for adsorption or degradation reactions [18]. This has consequences for drinking water quality, managing pesticides and nutrients in agriculture and even mining.

Fingered flow can be caused by water repellency, air entrapping, or as in this case, textural contrasts. These fingers persist over a long period [11]. Formed fingers can persist because with reapplication of water, the water will enter at the previously formed fingers. Hysteresis plays an important role in the persistence of flow fingers in sandy soils [11]. The initial water content in and around the flow fingers is important to know the width [16]. This has also been stated by [1]: the hydraulic properties and the amount and location of the preferred flow paths is a function of the mean saturation of the domain. The channels cause the solute to be dispersed more strongly, i.e., the dispersion is saturation dependent.

Roth and Hammel (1996) used a numerical model to explore how small-scale hydraulic properties relate to large-scale transport phenomena in heterogeneous unsaturated media [23]. They found that many of the encountered phenomena found in the field can be simulated by the model. These are for example the formation of isolated regions of high solute concentration, a global dispersion (averaged over whole domain) that is much larger than the local dispersion and flow that bypasses a large part of the matrix (Figure 1).

Furthermore they modelled the transition from effective stochastic-convective to an effective convective-dispersive process with increasing transport distance. In other words, in the beginning the transport is convection-based. The solute moves down with the moisture front and does not move with respect to the water (Figure 2). Spreading is then proportional to the travelled distance, because of the different distances passed. This can be described by the stochastic-convective transport model (SCM). Further away from the source, the dispersion is stronger and solutes spread also because of the concentration gradients in longitudinal and lateral directions. The convection-dispersion equation (CDE) describes this transport behaviour. This also becomes clear when picturing effective longitudinal dispersivity versus depth. The longitudinal dispersivity increases with depth, and at a certain depth it reaches a constant value, as is also used in the CDE. These two processes have also been described as the 'near-field' and 'far-field' behaviour [3, 34].

Another interesting phenomenon that appears in transport in heterogeneous media is found by Roth (1995). The complex hydraulic structure, resulting from the heterogeneity of the domain,

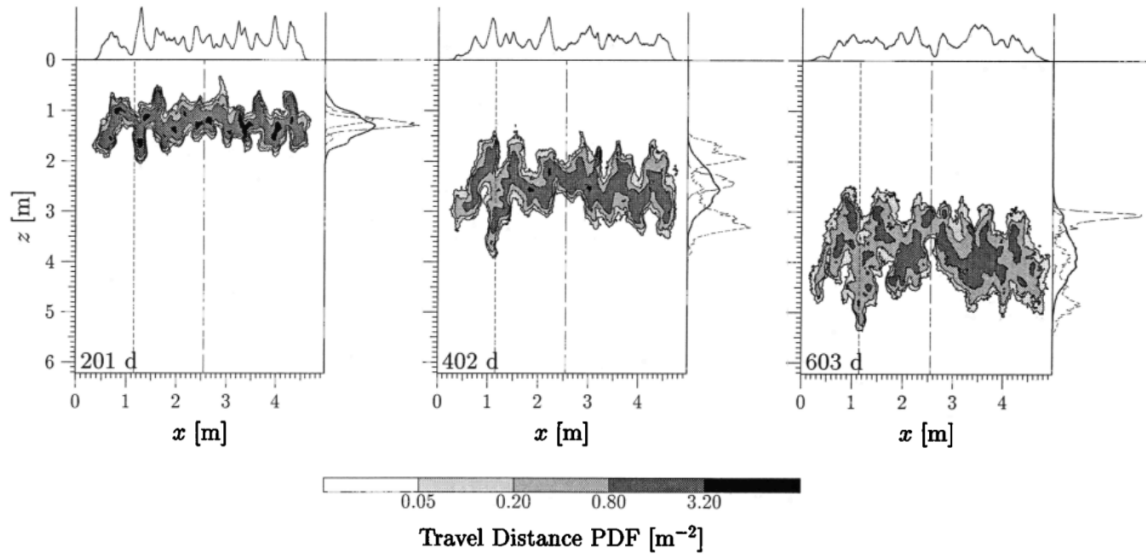


Figure 1: Probability density function (pdf) of travel distance for three moments of a conservative chemical during steady state flow. The curve at the top shows the vertically averaged particle positions. At the side, the solid curve indicates the horizontally averaged distributions and the dotted curve the distributions for the 'core' locations. From: [23].

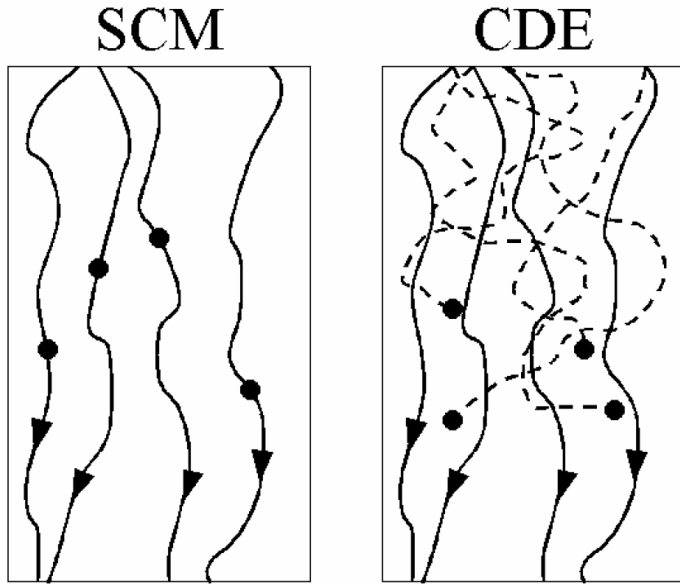


Figure 2: Solute spreading mechanisms: the stochastic-convective model (SCM), where solutes stay in the flow paths, and the convection-dispersion equation (CDE), where solutes move analogous to molecular diffusion. From [32].

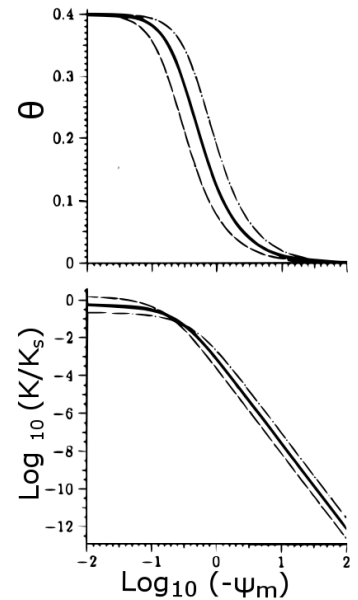


Figure 3: Hydraulic functions for the case pictured in Figure 4. Dashed line indicates a coarser medium, the dash-dotted line a finer medium. Adapted from [22].

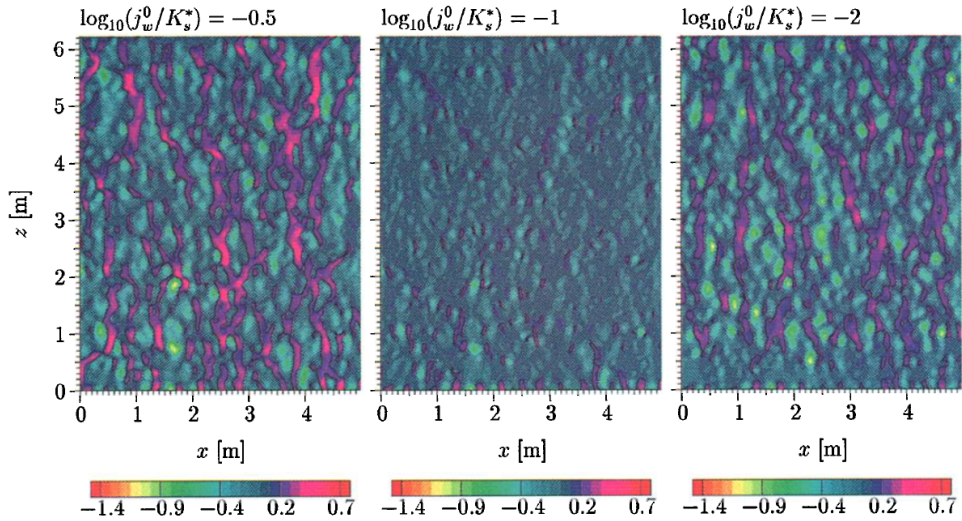


Figure 4: Dimensionless water flux for different values of the input flux (indicated above figure). From [22].

occurs in two states with clear flow channels that are separated by a critical point where the hydraulic structure disappears, but a more homogeneous flow field with a uniform flux is observed (Figure 4). These states are complementary, the high-flux regions in one field become the low-flux regions in the other field. Transition between these hydraulic structures is a function of saturation, i.e. at either high or low saturation the flow paths emerge [22]. It is the result of the fine-textured regions becoming more conductive than the coarse-textured regions in a dry situation, whereas in the wet situation the coarse-textured regions are most conductive (Figure 3).

From these previous studies some knowledge gaps can be identified. The numerical model of Roth and Hammel showed transport features as also found in the field, but it is still limited and could be further improved to make it more realistic [23]: in realistic situations, water flow is often transient. This may influence spreading processes due to different inflow timing and velocities. Especially during high inflow events (eg. during melt) steady-state simulations cannot predict contaminant transport well, underestimating leakage. Transient simulations, however, do show higher contaminant concentrations because of the short residence times and therefore reduced degradation and sorption [13].

Next to that, the existence of different hydraulic structures due to different saturation levels Roth found for steady state flow [22], as explained before, will also apply in case of changing inflow and influence spreading. In other words, when transient flow is used in a similar heterogeneous medium, flow paths are expected to shift, with the change in hydraulic structure. When we apply this to a case with solute transport, this will imply that the solute will shift with the flow sideways. In the new environments that are encountered there, different conditions could be found, influencing degradation and therefore breakthrough.

2.3. Root water uptake

In many solute transport models root water uptake is described in a simplified manner, e.g. by using effective infiltration as an input (*Precipitation – Evapotranspiration*). However, in the upper zone of the soil some important things happen: the larger precipitation flux is infiltrating and part of it is transpired by plants, where another part is evaporated at the surface already. It may be that the way of taking up water by the roots has an impact on the transport of chemicals,

spatially as well as temporally. For example, the decreasing water flux in the root zone will influence the velocity and the route of transport via the previously described shift in hydraulic structures [22]. Water uptake by rooting systems can control the timing and the amount of chemical pollutant loadings to the groundwater through elimination of preferential flow patterns of water and chemicals ([4], in [38]). As the roots take up water from the regions with a higher pressure head, the spatial distribution of water flow will be affected.

Models for root water uptake have not often been combined with contaminant transport in heterogeneous media. One of the few articles published on this is by Kuhlmann et al. (2011), who assessed numerically the effect of soil heterogeneity in combination with root water uptake on the variability of unsaturated flow. They found that simplified macroscopic models for root water uptake should be used with care in heterogeneous media, as local wilting regions can develop at coarse patches, which is a numerical artefact and no realistic situation. In reality, plants use compensation mechanisms, where roots take up more water from wet regions to compensate for the drought-stressed regions. This is also included in simulations to test the applicability.

Rubin and Or (1993) considered the case of RWU in a 1D column model, with heterogeneity in either the vertical or the horizontal plane [25]. Water uptake decreased exponentially with depth, following a model for root water uptake based on Raats (1974). They hypothesised that the effect of RWU may become significant in situations where rooting depth is of the same order of magnitude as the depth to the water table: in their simulations the pattern of the RWU as determined by rooting depth and ratio of transpiration and surface flux (T/q_0 , with T for transpiration and q_0 for surface flux) determined the portion of the domain over which pressure heads are stationary. With a large flux ratio or a large rooting depth in comparison to total depth, this stationary region in variance of saturation and matric potential may not exist at all [25].

Another study by Russo et al. (1998) investigated flow and transport in a heterogeneous domain in a 3D-simulation. Including root water uptake produced a profile with lower conductivity and a steeper head gradient. In this model, RWU decreased the spreading in the vertical direction and reduced the skewness of the concentration profiles because the water uptake by the roots eliminates the high vertical velocities and thereby smooths out its vertical heterogeneity. Solute spreading is consequently also less spread in the vertical direction [26].

It may be clear that root water uptake has a strong influence on solute transport. The objective of the this study is to find out more about these differences in modelling with and without root water uptake. Later, this could contribute to a method where the effect of root water uptake is realistically included into a simpler model, without having to include the detailed root water uptake processes.

3. Methodology

3.1. Model structure

3.1.1. Basic model

A model answering to this objective is set up by A. Dathe in Hydrus-2D. This code simulates the movement of water and solutes in variably saturated media, and uses the Galerkin finite element method and the Crank-Nicholson scheme for temporal discretisation [44]. The conceptual model consists of a domain of 5 m wide and 6.25 m deep, representing a soil with heterogeneity in conductivity, with a resolution of 500 by 625 cells. At the two vertical boundaries there are no-flow conditions, where at the bottom the pressure head is set to 0, representing the groundwater table. At the top boundary, there is a uniformly distributed inflow, changing over time, as will be elucidated later.

Transient flow in an unsaturated medium is described by the Richards' equation [45]:

$$\frac{\partial \theta(h)}{\partial t} = \frac{\partial}{\partial x_i} \left[K(h) \left(\frac{\partial h}{\partial x_j} \right) \right] - S \quad 1$$

where θ is the volumetric water content, h the pressure head (cm), x_i and x_j are the spatial coordinates (cm), t is time (h), K is the unsaturated hydraulic conductivity (cm/h) and S the sink term (1/h).

The unsaturated soil hydraulic properties, the soil water retention function $\theta(h)$ and the hydraulic conductivity function $K(h)$ are nonlinear functions of the pressure head. These relations are described by the Van Genuchten functions $\theta(h)$ and $K(h)$, with a pore size distribution described by Mualem [33]:

$$\theta(h) = \begin{cases} \theta_r + \frac{\theta_s - \theta_r}{[1 + \alpha h^n]^m} & h < 0 \\ \theta_s & h \geq 0 \end{cases} \quad 2$$

$$K(h) = K_s S_e^l [1 - (1 - S_e^{l/m})^m]^2 \quad 3$$

with

$$m = 1 - \frac{1}{n}, \quad n > 1 \quad 4$$

and

$$S_e = \frac{\theta - \theta_r}{\theta_s - \theta_r} \quad 5$$

where θ_r and θ_s are the residual and saturated water content, α is the inverse of the air-entry value (1/cm), n the pore-size distribution index, K_s the saturated hydraulic conductivity (cm/h), S_e the effective water content and l the pore-connectivity parameter. The medium considered here has the properties $K_s = 3.6$ cm/h, $\theta_r = 0$, $\theta_s = 0.4$, $\alpha = 0.04$ /cm, $n = 2$ and $l = 0.5$. The longitudinal dispersivity is set to 0.4 cm and the transversal dispersivity is 10 times smaller, i.e. 0.04 cm.

Transport of solutes during transient flow in a variably saturated medium is calculated by [45]:

$$\frac{\partial \theta C}{\partial t} = \frac{\partial}{\partial x_i} \left(\theta D_{ij} \frac{\partial C}{\partial x_j} \right) - \frac{\partial q_i C}{\partial x_i} - S c_r - \mu \theta C \quad 6$$

where C is the solute concentration (mmol/cm^3), μ is the first-order rate constant ($1/\text{h}$), q is the flux (cm/h), S is the sink term in Equation 1, c_r is the concentration of the sink term (mmol/cm^3) and D_{ij} is the dispersion coefficient (cm^2/h).

To simulate the heterogeneity of the subsurface, a reference state and a scaling factor are used. The scaling relation between the scaling factor α and the reference state $K^*(h^*)$ is described by [37]:

$$K(h) = \alpha^2 K^*(h^*), \quad h = \alpha h^*. \quad 7$$

where α is scaled according to a Miller-Miller similitude [17]. The parameters used for this stochastic field are a standard deviation $\sigma_{\log^{10}(\alpha)} = 0.5$ and a correlation length in x - and z -direction of 0.1 m.

For high and low flow, input fluxes of respectively 1.138 and 0.0036 cm/h are taken. These are extreme values, but they are chosen to simulate flow at two sides of the critical point in saturation that determines the flow structure. The critical point is described by $\log_{10}(j_w^0/K_s^*) = -1$ which in this case gives an input flux of 0.36 cm/h , where j_w^0 is the water flux and K_s^* the saturated hydraulic conductivity of the reference state [22]. The complementary cases are then $\log_{10}(j_w^0/K_s^*) = -0.5$ and $\log_{10}(j_w^0/K_s^*) = -3$.

The correct initial pressure heads for each simulation are taken from a long initialising simulation with equal influx. At certain time steps a conservative solute is added with a concentration according to the intensity of the flux, in such a way that the added total amount is 2 mmol/cm of precipitation. Particles are absorbed at the lower boundary and reflected at vertical boundaries. For the numerical solution, a mass balance error below 1% is aimed for.

3.1.2. Root water uptake module

The domain is similar to the already used one: a 2-dimensional, vertical region of 500 by 625 cm. The root zone is located in the upper 100 cm of the domain (FAO, for wheat [8]) and has a certain uptake distribution, as described after this. For simulations without root water uptake, the domain has the same proportions, but the root zone is not present in the upper meter.

Root water uptake is distributed over the domain according to the spatial root distribution. Vrugt (2001) formulates six different root water uptake distributions which can be used in Hydrus [38]. Wu lumped data from three root growth studies by fitting a third order polynomial to the pooled data. He found that the root distribution of maize and wheat is approximately linear [42].

Uptake is uncompensated, which means that lower uptake because of stress in dry regions is not compensated for by a higher uptake by the roots elsewhere. No solute is taken up by the roots. Maximum root water uptake takes place at the surface.

Root water uptake is represented in Equation 1 by the sink term S . The potential root water uptake is calculated by ([36]):

$$S_p(z) = b(z)L_t T_p(t) \quad 8$$

where S_p is the potential root water uptake rate ($1/\text{h}$), $b(z)$ the normalised water uptake distribution ($1/\text{cm}^2$), L_t the width of the soil surface associated with the transpiration process (cm), T_p the potential transpiration rate (cm/h), z is the spatial coordinate.

Here the root distribution model of Raats (1974) as formulated by Vrugt (2001) is used:

$$b(z) = \left(1 - \frac{z}{Z_m}\right) e^{-\frac{p_z}{Z_m}|z^* - z|} \quad 9$$

where $b(z)$ is the dimensionless root water distribution, Z_m the maximum rooting depth, and p_z and z^* are empirical parameters. The root uptake distribution model integrates to 1 over the root zone.

A first control plane is located at the bottom of the root zone, a second one near the groundwater table, above the capillary fringe. Using these imaginary horizontal planes in the domain, the passing solute can be tracked. The location of the second control plane follows from previous simulations, and lies at $z=35\text{cm}$. The measure of root water uptake can then be obtained by looking at the solute arrival at these two levels.

Parameters for the first order degradation are chosen to let $0.1\ \mu\text{g}$ of the total applied mass ($100\mu\text{g}$) leach out at control level 2 in the basic scenario, according to the EU constraints on leaching [6]. Differences in leached amount can then be compared to see what would have been the effect in terms of EU formulated pesticide exceedance levels.

Output scenarios of this model with root water uptake can then be compared with the output of a similar but simplified model, i.e. no root water uptake in the upper region, and instead a decreased water input at the upper boundary ($q^* = q - T$, where q is the influx of the RWU model and T transpiration). The first control plane will still be present at the same location.

3.2. Scenarios

3.2.1. Preferential flow scenarios

To explore the processes taking place, a set of scenarios is worked out. The detailed input of these model simulations can be found in Appendix A.

1. First, simulations are done with steady state flow, to obtain the initial pressure heads for the subsequent simulations. This is done for a high (H) and low (L) input flux, where high and low refer to flow rates above and below the critical point determining the flow structure. Next, in this steady state flow scenario, a pulse of conservative solute is added (H1 and L1). From these steady state simulations we will also be able to see the developed flow channels, and how they differ in the two simulations. These channels will show up in the spatial distribution of the velocity, flux and of course the spreading of the solute. Furthermore, these simulations will serve as a reference to compare with the other simulations.
2. Then a set of scenarios with changing flow is considered: the time span is divided into two periods, one with high and one with low flow. With a solute added at $t = 1$ this gives the simulations HL1 and LH1. The aim of these simulations is to see how the changing flow influences the spreading of the solute. Next to that, the output of water content and velocity fields will show the development of moisture front and channels.
3. Similar to the previous scenarios, two simulations are considered where the second solute is added at the moment of the change in flow intensity in the simulations HL2 and LH2. The second solute is applied with the water with either a lower or higher intensity. This will show the movement of the second water front and its interaction with the previously applied solute pulse.

When only the second solute pulse is considered, a comparison with the steady-state simulations H1 and L1 (where the solute is added at $t = 1$) can be made. The applied input water will be the same, but the initial soil moisture content will differ. This will show the influence of the initial conditions before the switch to either higher or lower flow.

3.2.2. Root water uptake scenarios

1. A set of sub-scenarios with different values for the precipitation and evapotranspiration considers the domain in successively drier situations. Realistic ranges of precipitation and

evaporation values are taken from the KNMI [24].

Table 1: Yearly precipitation and evapotranspiration values for a set of scenarios.

P (mm)	ET (mm)	P-ET (mm)
700	550	150
850	550	300
1050	550	500

2. The inflow at the atmospheric boundary can be chosen such that the saturation in the upper zone is above the critical point, and the saturation below the first control plane below this critical point in saturation. An interesting shift in solute transport could then be anticipated.

The critical point in saturation at which the hydraulic structure changes is reached with a flux of $\log_{10}(j_w^0/K_s^*) = -1$. To obtain two complementary states at either side of this point, an initial infiltration of 0.4 cm/h is chosen, and an evaporation of 0.1 cm/h, corresponding to fluxes of resp. $\log_{10}(j_w^0/K_s^*) = -0.95$ and $\log_{10}(j_w^0/K_s^*) = -1.08$.

3. To obtain an impression of the influence of the depth of the unsaturated zone in comparison to the depth of the root zone only, a set of simulations will be set up with a shallower groundwater table, i.e. at -4 and -2 m instead of the -6.25 m in the basic simulation. The stochastic fields for conductivity and pressure heads have been cut and have therefore exactly the same structure in the upper part of all these simulations.

3.3. Analysis

To analyse the output of the modelled scenarios, a postprocessor of A. Leijnse is used [14]. The sides of the output fields are cut off before analysis to eliminate boundary effects: 25 cm on both sides and the top and 100 cm at the bottom. The cutoff at the bottom is larger than for the sides, because these boundary effects are especially present at the bottom at a flux below the critical value (see Figure 6). Near the groundwater table at the capillary fringe, the soil moisture increases, and a transition occurs where first a uniform flow, and even further down a phase-shifted flow structure can be seen. The critical flux of $\log_{10}(j_w^0/K_s^*) = -1$ is then passed.

For selected time steps a set of statistics is calculated. Spatial moments show the development of the infiltration front, by giving the location of the centre of mass (1st moment) and variance (2nd central moment).

To quantify the spatial structure of the flow paths objectively and compare the spatial correlation for different fields, variograms in x -direction are made. The variogram statistics (i.e. correlation length and corresponding variance) for all output fields (v , K , h , θ , C , θC and q ($=\theta v$)) are determined by fitting the variogram exponentially. This theoretical model is described by:

$$\gamma = \sigma^2 (1 - e^{-\frac{d}{a}}), \quad 10$$

where σ is the standard deviation, d the lag distance and a the correlation length.

From the variograms of velocity, C and θC , the size of the flow fingers can be derived. This can be done because the variograms show a hole-effect, i.e. an oscillating behaviour, which indicates a form of cyclicity or periodicity [19]. In the output figures we obtain, these are the

channels and other spatial structures. The variogram interpretation is illustrated in Figure 5. At the right a simplified output field of e.g. concentration, at the left the derived variogram which shows cyclicity. In the variogram, the distance to the first peak gives the smallest distance of non-correlation, an indication of the width of the flow finger (X_{mean} in Figure 5). The distance to the first trough is an indication of the width of a flow finger and an adjacent no-flow zone together (Y_{mean} in Figure 5).

Values for these distances are obtained using the postprocessor, where variograms are fitted with a wave-variogram. This theoretical model fit is described by:

$$\gamma = \sigma^2(1 - \frac{a}{d} \sin(\frac{d}{a})), \quad 11$$

where σ is the standard deviation, d the lag distance and a the correlation length. The wavelength for this variogram is $2\pi d$. Fitting is done for one z -level, in this case around an arbitrary level of $z = 450 \text{ cm}$. Fitted variograms are weighted using the amount of data-pairs. This is done for a maximum lag distance up to 450 cm and a maximum lag distance of 50 cm . However, due to a lack of information, sometimes no convergence could be reached for the wave-variogram fits. Therefore, some values are missing.

The correlation lengths of all output fields are determined, to compare this to the correlation length of the input scaling relation α (10 cm). Locating the front has been done by fitting an exponential curve and then looking for the e -folding distance. Again, variogram fits are weighted with the amount of data-pairs. A maximum lag distance of 450 taken, except for certain fields, where a maximum considered lag of 50 resulted in a better fit. These are indicated by an asterisk.

Furthermore, the position of the water front is determined by the postprocessor. Values between 50 and 600 are used to eliminate boundary effects. This is done by assuming that the curve for mean water content for each z is shaped like an error function, i.e. an integrated normal distribution with mean z_f and standard deviation σ_f . The theoretical water content at position z is then given by [14]:

$$\theta_z = \theta(-\infty) + \frac{\theta(\infty) - \theta(-\infty)}{2} \left(1 + \operatorname{erf} \frac{z - z_f}{\sigma_f \sqrt{2}} \right) \quad 12$$

where $\theta(-\infty)$ and $\theta(\infty)$ are the values for the function at $z = -\infty$ and $z = \infty$, lying between the residual water content and the saturated water content. The output water content values from Hydrus are fitted using this equation to give the depth of the water front.

Analysing root water uptake will be done by looking at total, spatial and temporal distribution of solute at the control planes. To find the leached mass, the total solute flux across the control planes can be tracked. Total masses in solution have been calculated by multiplying concentration

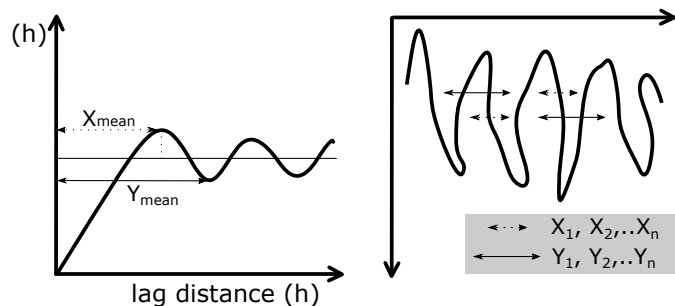


Figure 5: Infiltration front and corresponding variogram with interpretation

and saturation at these levels. When we compare this for a case with and a case without RWU, we will see if there is a difference. Total mass crossing the control planes can be plotted versus time to produce a breakthrough curve. The spatial distribution of the fluxes across the control planes follows from the output graphs of Hydrus itself.

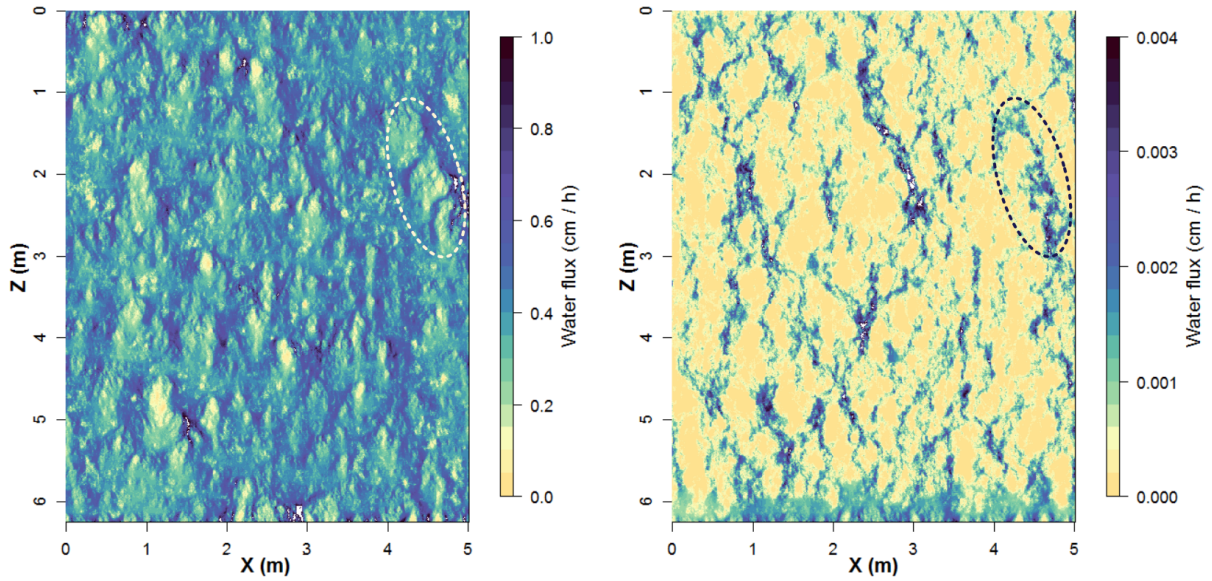


Figure 6: Output figures from Hydrus: water flux fields (θv [cm/h]) for the scenarios H1 (left) and L1. Yellow indicates low velocities, blue indicates high velocities.

4. Results and Discussion

4.1. Quantification of preferential flow paths

The preferential flow paths can be identified well from the output pictures (Figure 6). Steady state high and low flow (H and L) clearly show different hydraulic structures in the water flux-fields. These are the complementary states found before by Roth [22], which are easy to identify in the highlighted area. It is the result of the fine-textured regions becoming more conductive than the coarse-textured regions in a dry situation, whereas in the wet situation the coarse-textured regions are most conductive.

The flow paths seem to be more pronounced and connected in case of low input flux, with an apparent larger correlation length in the water flux fields (Figure 6). For the concentration fields the found correlation length for a transect at $z = 450$ is indeed larger for L1 than for H1, even more than twice as large (Table 2), whereas when we compare the correlation lengths for Darcy velocity (θv) and the total mass (θC) between the two flow situations, we see that the differences are negligible.

The values of θC can be explained by the differences in correlation length between the two cases for θ , which is smaller for the low-flow case. This compensates for the larger correlation length for concentration, and together they result in the similar values for θC in case of low and high flow. However, for θv this does not hold.

The differences in correlation length for the solute concentration C have a strong link to the differences in (interstitial) velocity v , as this determines the transport of the solute. The correlation length for C is larger for the low flow case than for the high flow case. However, this cannot be traced back to a larger correlation length for velocity in the low flow case compared to the high flow case.

The variances of the output fields in Table 2 are not easy to compare, as the means of these fields are very different. A better measure of comparison is the dimensionless coefficient of variation. In general, the relative variation is small for p and θ , as values for θ are limited between

0 and the saturated water content. The coefficients of variation for the concentration-fields C and θC are larger due to larger variability in concentrations in relation to the mean that are present in the output-fields.

When comparing the two flow cases, it becomes clear that C , θC and pressure-fields are comparable in their relative variation. For the other parameter fields, v , θv , θ and k , the differences are clear: in all four cases, the relative variation is 2 to 7 times larger in the low-flow situation than in the high-flow situation.

As mentioned before in the Literature Review, Roth (1995) modelled similar situations [22]. A series with different input fluxes was considered, to obtain saturations higher, lower and equal to the critical point. At this critical point, the hydraulic structure disappeared and a uniform flux was observed. With increasing distance from this critical point (higher or lower saturation), the network of flow channels became better connected and more pronounced, i.e., the flux ratios between high- and low-flux regions increased.

The same is found by Birkholzer and Tsang (1999). They pictured the spatial distribution of relative flow rate for four unsaturated cases. They also found the most obvious channelling effects at the low-infiltration case, with increasingly homogeneous flow pattern and less variation in effective permeability for flow cases with an increasing saturation towards the critical point [1].

When we compare these outcomes to our results, we see the clearer flux for the low-infiltration case (which lies further away from the critical point) compared to the high-infiltration case that has also been found before. The intermediate case or more extreme cases at either side of the flow regimes have not been modelled.

Concerning the alignment, Roth found that flow channels for the highest input flux are more aligned with the vertical than are those for the smallest fluxes. He could not answer if this was a feature of a particular realisation or a more general property. Opposed to what Roth found, Birkholzer and Tsang found that the alignment was better in the intermediate cases, but cases with extremely low and high infiltration dealt with horizontal flow because of low-permeability blocks that had to be overcome. In the output fields of this study, no clear difference can be seen in the vertical alignment. Of course, these two realisations are too limited to compare them to the results found in the aforementioned studies. We cannot extrapolate the found patterns to know if the vertical alignment changes in intermediate cases or in more extreme high- or low-infiltration cases.

At the bottom a transition zone can be seen, where the channels disappear and a uniform flow occurs, with a smaller variance in flow. This is a result of the saturation which increases and passes the critical point. The hydraulic structure changes consequently. Therefore, this zone does not show up at the high input flux situation, where the saturation is already high.

The occurrence of this transition near the capillary fringe has been reported before in literature [1, 22, 25]. For example, a similar situation to this transition zone has been described by Rubin and Or (1993). For a stochastic parallel columns model they found a region near the water table where the pressure head variance is practically zero. The extent of this region became larger at a lower input flux.

To quantify the spatial structure of the preferential flow paths in a more objective manner, variograms are made of the following fields, for a depth of $z = 450\text{cm}$: v , q ($=\theta v$), K , h , θ , C and θC . The correlation lengths of all these output fields have been determined, to compare this to the correlation length of the input scaling factor α (10 cm) and to see how this input factor works through in the output fields.

The resulting values can be seen in Table 2. In comparison to the scaling parameter, quite deviating values show up here. For most fields, the correlation lengths are smaller than for the scaling parameter (θ , v , θv , θC , C and K). The equations on which these parameters depend,

Table 2: Correlation lengths for variograms along $z = 450\text{cm}$ and coefficients of variation of the stationary fields $H1$ and $L1$. Variogram fits with max. considered distance of 50 cm indicated by *.

H1, $t = 3250h$	Correlation length (cm)	Variance	Coefficient of Variation (-)
v	4.86	8.36×10^{-6}	2.95×10^{-1}
θv	4.80	1.31×10^{-2}	3.05×10^{-1}
C	6.79	3.21×10^{-3}	3.31
θC	6.86	3.93×10^{-4}	3.36
θ	8.04	2.60×10^{-3}	1.27×10^{-1}
p	19.6	2.00	2.28×10^{-1}
K^*	5.90	7.03	7.47×10^{-1}

L1, $t = 26000$	Correlation length (cm)	Variance	Coefficient of Variation (-)
v	3.25	8.85×10^{-2}	6.59×10^{-1}
θv	4.31	4.73×10^{-6}	1.02
C	14.3	1.61×10^{-2}	3.11
θC^*	6.12	3.86×10^{-4}	3.45
θ^*	5.42	3.26×10^{-3}	5.50×10^{-1}
p	22.0	45.1	2.38×10^{-1}
K	4.45	1.17×10^{-3}	5.79

such as the retention function and the hydraulic conductivity function, add heterogeneity to the scaling field, in the sense that the spatial patterns are finer here.

Birkholzer and Tsang [1] stated that the infiltration rate indeed not only changes heterogeneity but also spatial correlation. This applied to the correlation length of the effective permeability, which for low and high-flow case was similar to the input value chosen for the random field, but in intermediate cases (in terms of infiltration amount) the correlation length was found to be less.

The larger correlation length for the low flow concentration field in comparison to other fields could also be explained by the way the solute is infiltrating. At the top of the domain, the solute is applied homogeneously. It will infiltrate quicker at locations with high hydraulic conductivity, these regions being determined by the spatial structure of the medium (the random field). Further away from the surface, it is not only the conductivity determining the structure of the flow paths. When a region with lower conductivity is encountered, the flow is diverted or the pressure builds up until the flow continues through this region. These processes result in a coarser, irregular and anisotropic pattern for solute concentration than observed for total mass, conductivity, velocity, flux and moisture content fields.

It becomes clear that the concentration output field cannot be related directly to the other parameter fields, and is therefore harder to predict. Implications of this are that the spatial structure of the scaling factor, i.e. the heterogeneity of the soil, which would be measured in the field normally, should be used with care when predicting the spatial pattern and correlation lengths of solute transport processes in certain cases with low infiltration rate.

From the variograms of θv , C , θC , θ , p and K the structure of the spatial pattern has been derived. The resulting values can be seen in Table 3, and these are quite divergent for different fields and flow velocities. For the fields of C and θC , these indicate the size of the flow fingers. Their horizontal width is, for the high-flow case, about 50 cm. This agrees with the output pictures (Appendix B).

A graph showing the centres of mass versus x for the two scenarios (H and L) for a time step for which the solute front has moved to a comparable depth, will show an inverse pattern to

Table 3: Variogram analysis giving the lag distance and variance for the first peak and through of each variogram for $z = 450\text{cm}$. C and θC values for L1 missing because there was no clear fit possible. Values are found using the horizontal tangent for the first top and through.

H1, $t = 3250h$	A mean		B mean	
	Distance (cm)	Semivariance	Distance	Semivariance
θv	10	1.19×10^{-2}	14	1.12×10^{-2}
C	50	4.47×10^{-3}	97	2.10×10^{-3}
θC	51	6.27×10^{-4}	82	3.11×10^{-4}
θ	25	2.72×10^{-3}	46	2.3×10^{-3}
p	43	2.37	78	1.72
K	29	8.95	46	7.03

L1, $t = 26000h$	Distance	Semivariance	Distance	Semivariance
θv	18	5.28×10^{-7}	51	6.32×10^{-7}
θ	25	3.55×10^{-3}	46	3.00×10^{-3}
p	52	4.81×10^{-1}	91	3.57×10^{-1}
K	23	2.10×10^{-3}	48	1.60×10^{-3}

a certain extent (not shown). Where the solute has moved further with high flow, it has moved less for low flow and vice versa. This is again the result of the fine-textured regions becoming more conductive than the coarse-textured regions in a dry situation. The inverse pattern does not become more clear in the graph with increasing depth. In the spreading of the solute more things are taken into account than only the preferential flow paths itself: i.e. how the solute has spread in the time before. However, when a similar figure is made, plotting the velocity at a certain depth z versus x , this gives a clearer inverse pattern (Figure 7), because it does not take into account the ‘history’ of flow paths. Therefore the differences are less evened out and clearer to see.

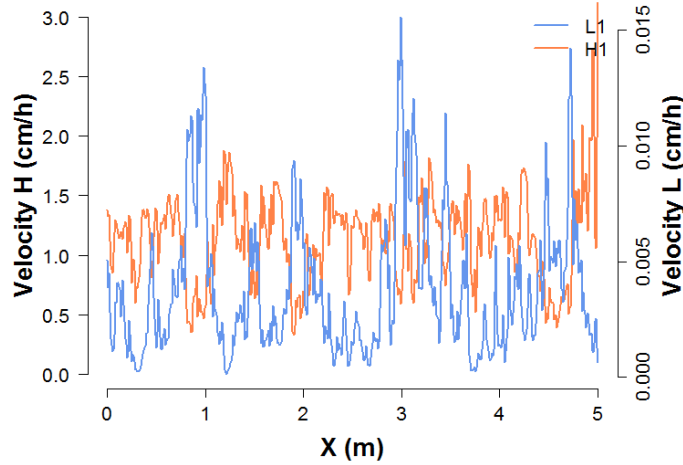


Figure 7: Velocity of the flowpaths at $z = 400\text{cm}$ for high and low flow.

4.2. Influence of initial conditions on flow pattern

To test the influence of initial conditions, simulation H1 has been compared to a simulation LH2 where now only the second solute is considered. The difference between these simulations will show how the previous lower (or higher) flow can influence how the solute is spreading.

The difference in mass between these two simulations is plotted in Figure 8 ($LH2_{tracer\ 2} - H1$). The difference in mass in solution is quite substantial (until 0.03 mmol/cm³ on a total concentration of max 0.07 mmol/cm³), but very localised. On certain spots (mostly at the top of the front) the concentration is higher in simulation LH2, where at the bottom of the front the concentration is lower in simulation LH2 than simulation H1. This can be seen at both shown time steps. The low flow initial conditions, represented in simulation LH2, make that the front is lagging behind slightly compared to the front with high flow initial conditions.

However, with a higher initial water content we would expect the water front to be quicker, because less unoccupied pore space has to be filled, and the solute front to be uninfluenced. Apparently, this is a too simplistic view.

A better explanation can be found in the initial low pressures. The average pressure head for the low-flow case is -76 cm, where the high-flow case has an average pressure head of -10 cm. Before the high flow water front, including the solute, can continue to move further, the pressure has to build up. After some time, the water front is then moving down with its high velocity, and the solute follows later (see subsection 4.4). In Figure 9 the effect of this initial low pressure can be seen. It is not very clear, but the orange line, indicating movement of the solute with high flow initial conditions, moves downwards steadily. The line indicating low-flow initial conditions, however, first moves down slightly slower, to make a bend and later moves down parallel, with the same speed, as in the other case. This gives an impression of how the initial low pressures influence the movement of the solute down.

The same concentration difference calculations are done for L1 and $HL2_{tracer\ 2}$. Here, no large differences appear. The difference in mass in solution between the two fronts is limited (until 0.01 mmol/cm³ on a total concentration of max 0.1 mmol/cm³). Also, this difference appears over the whole front, and not locally. The initial high-flux conditions make the front to have a slightly higher concentration. It is not clear yet what could be causing this.

Experimentally and in the field, this issue of influential initial conditions has also been studied. Flury [7] studied the effect of initial soil water content on the penetration depth of dye in 14 different field soils. It seemed that for most cases the dye moved slightly deeper into initially dry soil, but the found differences were too small to draw conclusions. White et al. [41] carried out a similar field study for a clay soil, and found more leaching for chemicals under initially dry soil conditions. On the other hand, the results of experiments by Steenhuis and Muck [30] suggest that pesticide leaching (through macropores on a silt loam hill slope) is smaller in initially dry soils, as the water is drawn into the smallest pores by matrix potential. It may be clear that the effect of initial soil moisture content on solute transport in the field is not yet agreed on.

In short, for low flow initial conditions before a high-flow event, the solute has been shown to move down slower than with high-flow initial conditions. This may be caused by the need for building up the pressure to let the flow continue in the high-conductivity flow paths. For the opposite case, high-flow initial conditions followed by a low-flow event, no clear pattern is observed, but a small difference in mass is seen. The reason for this, however, is unclear still.

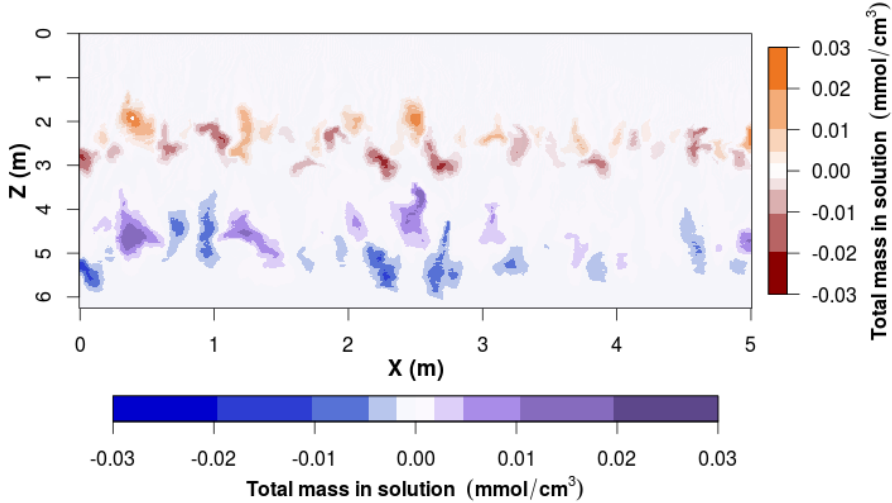


Figure 8: Difference in mass in solution for the simulations H1 and LH2_{tracer2} ($C_{LH2\text{-tracer2}} - C_{H1}$) at 75 h (red) and 150 h (blue) after the application.

4.3. Solute spreading behaviour under transient water flow

The model has been run as explained in the Methods section: LH2 stands for a simulation where the solute is added at the first time step, and where, as soon as the first solute front is halfway the domain, the flux is changed and a second solute is added with high flow. A figure with the centres of mass is made for the two solutes in one graph (Figure 10). This is pictured for times as indicated in the figure. From the figure it becomes clear that the second solute front is quicker than the first one. The red line, picturing the centres of mass of the second solute, catches up with the blue line. The graph just shows the centres of mass, but in reality there is a plume of solute around this. These solute plumes are overlapping and mixing due to dispersion (Figure 11).

Another thing that becomes clear from the picture, is the agreement between the grey line and the first solute front at $t = 6135$ h (Figure 10). The grey line indicates the location of the centre of mass of a solute applied in steady-state high flow conditions, simulation H1. This line has been pictured to show that after the regime shift, the solute applied in low flow moves towards the high-flow channels. Because of the agreement between these centre of mass-distributions we can deduce that the solute, which was previously located in low flow-high conductivity regions, moved to high flow-high conductivity regions.

When the moisture front of the high flux approaches the first solute front, this solute is compressed vertically. The tracer fills a smaller vertical space then before, as can be seen in Figure 12a. Later, with the passing of the moisture front, the solute front spreads out again. This also becomes clear from the position of the centres of mass and the variance at certain time steps (Figure 12b, detailed view in Appendix B, Figure 21). At first, the low flux moves the front down steadily, while the variance increases, as expected. At the shift, the variance becomes less, indicating the compression, while the front continues moving down with the same speed. Only after this compression, the front moves down with the high flux, as can be seen in the graph. The mean centre of mass makes a steep decline and the mean variance increases again.

For the opposite case, HL2, a high flux followed by a low one, the above mentioned is not

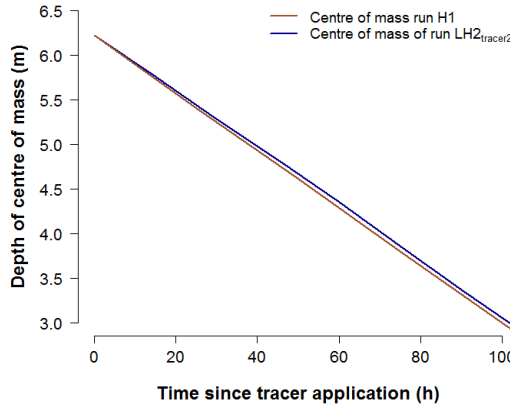


Figure 9: Movement with high flow of the centre of mass of a solute in high and low flow initial conditions.

the case. After the shift, the first solute continues moving down with a high velocity, while the second solute moves with the speed of the low flux (Figure 12c). Mixing, or even taking over, of the two solutes will therefore not happen in this case. The first solute front shows another feature again here: as part of the solute front lags behind and ends up in the low flow, the spreading increases (Figure 12d). This additional increase of dispersion can be explained as follows: as a starting point, we know the total mass θC_z in the domain has to stay equal (as long as all of the solute is still present above the groundwater). Then, as the low-velocity water follows up the high-velocity water, the amount of solute does not change, but the moisture content decreases. Therefore, the depth over which the solute is spreading has to increase.

The processes shown here become important in the view of infiltrating pesticides and degrading chemicals. The first finding, overlapping fronts, could imply that chemical concentrations increase locally. With given parameters for degradation, e.g. microbial biomass and electron acceptor availability, this could cause a slower or limited degradation. Higher fluxes taking chemicals previously captured in the low-flux flow paths increase leaching.

On the other hand we have the second process, where the first solute front is increasingly spreading. This order of flow regimes, low following high, increases travel times of the chemical in the unsaturated zone. This is positive as it increases potential for degradation and decreases leaching to the groundwater.

These results can be related to previous findings in [34]. In an overview paper, Vanderborgt et al. discuss transport in non-stationary flow fields and the effect of transient flow regimes on transport in a heterogeneous soil profile. In a 3D-simulation of solute transport in a heterogeneous domain, increased lateral solute redistribution from regions with high flow rates to regions with lower flow rates were observed in transient simulations. This larger lateral mixing decreased the vertical spreading ([26]). This could be similar to the mixing solute fronts pictured, where solutes are laterally redistributed from low- to high-flow paths.

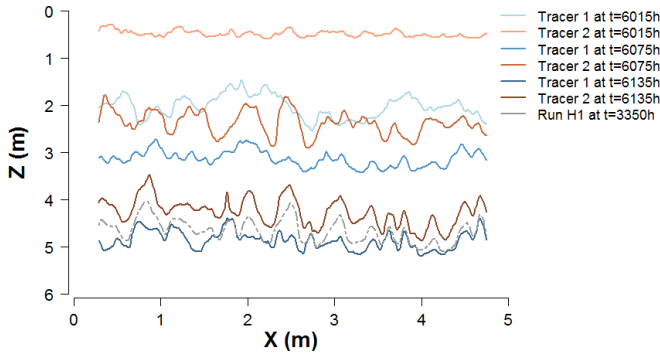


Figure 10: Centres of mass of two solutes for simulation LH2, where solute 1 (blue) is added at $t=0$ with low flow, and solute 2 (red) is added at $t=6000h$ at the shift to high flow. Grey line indicates the centre of mass of simulation H1, 150h after application.

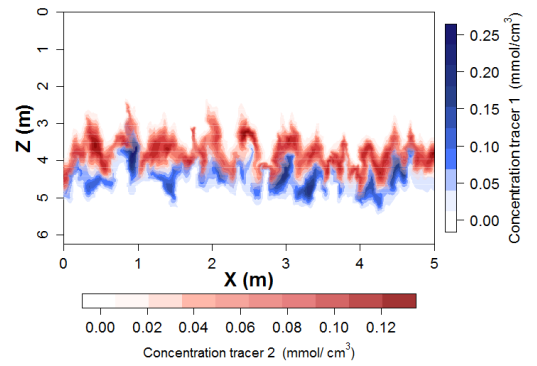
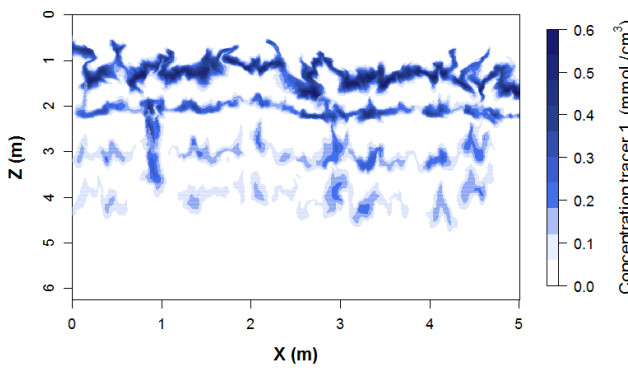
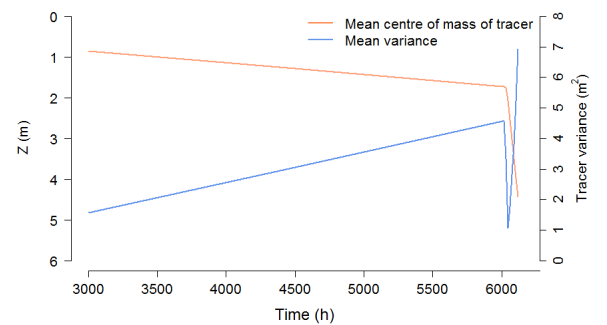


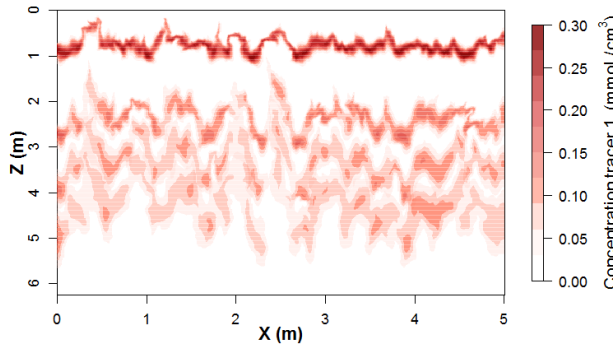
Figure 11: Simulation LH2 at $t=6120h$. Solute 1 (blue) is injected at $t=0$, solute 2 at $t=6000$, with the shift to high flow.



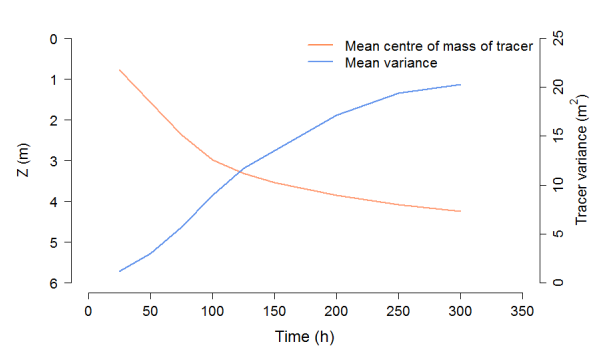
(a) Low flow followed by high flow (LH2, first solute shown). solute fronts given for $t=4500, 6045, 6075$ and $6105h$. Shift to high flow occurs at $t=6000h$.



(b) Depth of the centre of mass of the solute and its variance for the case LH2, solute 1. Shift to high flux at $t=6000h$. For a detailed view see Appendix B.



(c) High flow followed by low flow (HL2, first solute shown). Solute fronts given for $t=25, 75, 125$ and $300h$. Shift to low flow occurs at $t=75h$



(d) Depth of the centre of mass of the solute and its variance for the case HL2, solute 1. Shift to low flux at $t=75h$

Figure 12: Solute infiltration for the cases LH2 (top) and HL2 and corresponding graphs.

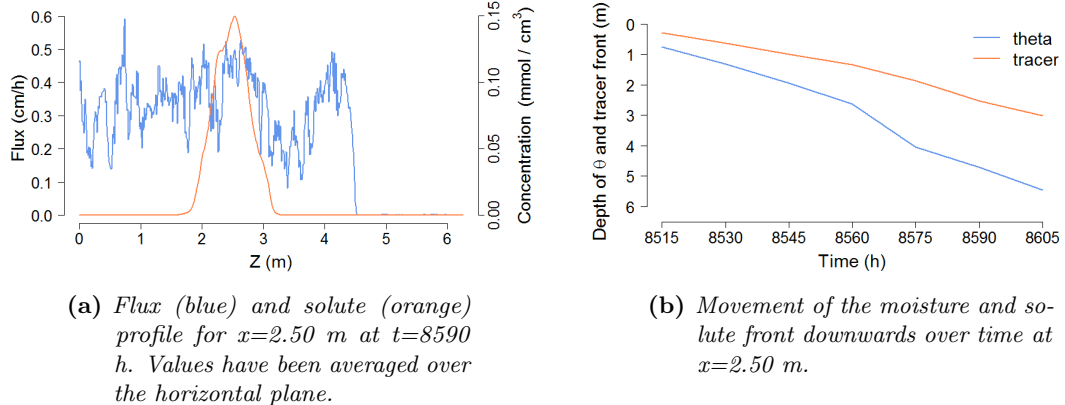


Figure 13: Relation between the flux-front and the concentration front shown for a single and multiple time steps for the case LH1.

4.4. Differences in movement of solute- and water front

When the displacement of the water front is compared to the solute front a striking phenomenon appears: the water front is quicker than the peak of solute moves down. In Figure 13a this effect is shown, where the water flux and solute peak (θv and C) move from low to high values of z , and in Figure 13b this is plotted for each time step.

The solute front lagging behind on the water front could be explained by the difference in space the water resp. solute has to fill. The domain is already partly saturated and when the high water flux moves down, only the unoccupied space has to be filled. However, when the solute front encounters the new region, it has to spread over the available pore water and the new water, i.e. the total porosity. This only holds for a situation where low flow is followed by high flow (LH1), and not for the opposite case (HL1). In the latter situation, a step to lower saturation instead of higher saturation is made, and therefore no similar situation occurs.

The difference in displacement has been described before in field and experimental cases and can be quantified by calculating the infiltration front velocity c and solute front velocity v . For conditions of steady flow through the unsaturated zone, with unit hydraulic gradient, and thus simplified, the kinematic velocity of the infiltration front (also called the celerity) can be expressed as [21]:

$$c = \frac{dK}{d\theta}, \quad 13$$

where dK is the difference in mean unsaturated hydraulic conductivity before and after the passing water front and $d\theta$ the difference in soil moisture content. The solute velocity, v , may be calculated by the following equation:

$$v = \frac{K}{\theta}. \quad 14$$

with values for K and θ for the latter condition, after the passing of the water front. The ratio between these two velocities is the kinematic ratio:

$$k = \frac{c}{v}. \quad 15$$

This difference in pressure-wave velocity (celerity) and advective velocity of a conservative solute is substantial, for theoretical and experimental cases until 15 respectively 1000 [21]. The kinematic ratio for this case amounts to 1.5.

Warrick describes in 1971 how the solute front lags behind on the water front and notes the relatively limited influence of the initial moisture content, but the high influence of the moisture content kept at the soil surface [39]. Solute distribution advances with $K(\theta_{wet})/\theta_{wet}$ where the faster moisture front was described by $K(\theta_{wet})/(\theta_{wet} - \theta_i)$, similar to the previously formulated equations.

In this model (Figure 13), including preferential flow, we indeed see that the pressure velocity is quicker than solute velocity. Where Raats [20] defined this ratio of water and solute velocity for uniform soils with an initial uniform water content, the different velocity of pressure front and solute front clearly also takes place in non-uniform cases. However, for the current situation these equations may be an oversimplification, as the domain is not uniformly saturated.

4.5. Precipitation-evaporation series including root water uptake

In Figure 14a the breakthrough curves (BTCs) over the first control plane (CP1) can be seen. For an overview of the boundary conditions, see Table 1.

The smaller the effective infiltration, the longer it takes for the solute to break through. Because the simulations all have the same degradation constant, this means that the later the breakthrough is timed, the lower is the total solute amount. Values for total mass passing each control plane can be found in Table 5. This effect is most clear for the BTC's and total masses passing control plane 2 (Figure 14b).

The dashed curves show results of the simulations without root water uptake but with the same amount of effective infiltration (i.e. below the root zone towards the groundwater). In all cases, these curves have lower peaks and surfaces than the curves indicating root water uptake. Also, the breakthrough starts later and the BTC's of cases with root water uptake are more skewed than the dashed curves, especially in Figure 14a. Continuous curves are broader than the dashed curves.

In cases with root water uptake, the infiltration velocities are higher in the upper part of the profile, where the roots have not taken up all water yet. This results in a quicker breakthrough and therefore less degradation. This explains both the lower peaks, the smaller surface and the later breakthrough of curves showing simulations without root water uptake. The broader curves in case of root water uptake can also be explained, as higher velocities imply more dispersion, which is velocity-dependent.

Table 4: Peak values and times for graphs shown in Figure 14.

BTC $P - ET$ (mm/y)	CP1		CP2		
		peak value (mmol/cm ³)	time (h)	peak value (mmol/cm ³)	time (h)
500	with RWU	8.29	1750	7.26×10^{-2}	12000
	without RWU	2.50	2200	1.63×10^{-2}	12500
300	with RWU	1.21×10^1	2400	1.30×10^{-2}	17250
	without RWU	1.03	3100	2.94×10^{-3}	18000
150	with RWU	3.15	3300	2.24×10^{-4}	27000
	without RWU	2.70×10^{-1}	5000	3.25×10^{-5}	29000

Table 5: Total mass in solution passing control planes for all simulations [mmol/cm³]. For a detailed description of simulations, see Appendix A.

	CP1	CP2
RWU ₂	6.35×10^3	4.22×10^3
RWU ₄	6.06×10^3	5.42×10^2
RWU PET150	5.97×10^3	1.11
RWU PET150 _N	6.79×10^2	1.79×10^{-1}
RWU PET300	5.96×10^3	3.93×10^1
RWU PET300 _N	1.59×10^3	1.17×10^1
RWU PET500	6.65×10^3	2.15×10^2
RWU PET500 _N	2.57×10^3	4.95×10^1
RWU Shift	7.16×10^3	1.63×10^2
RWU Shift _N	5.95×10^3	7.78×10^1

Table 6: Ratio of total mass in solution leaching over CP1 and CP2 based on previous table. Ratio as situation with RWU / situation without RWU.

	CP1	CP2
RWU PET150 / RWU PET150 _N	8.8	6.2
RWU PET300 / RWU PET300 _N	3.8	3.4
RWU PET500 / RWU PET500 _N	2.6	4.3
RWU Shift / RWU Shift _N	1.2	2.1

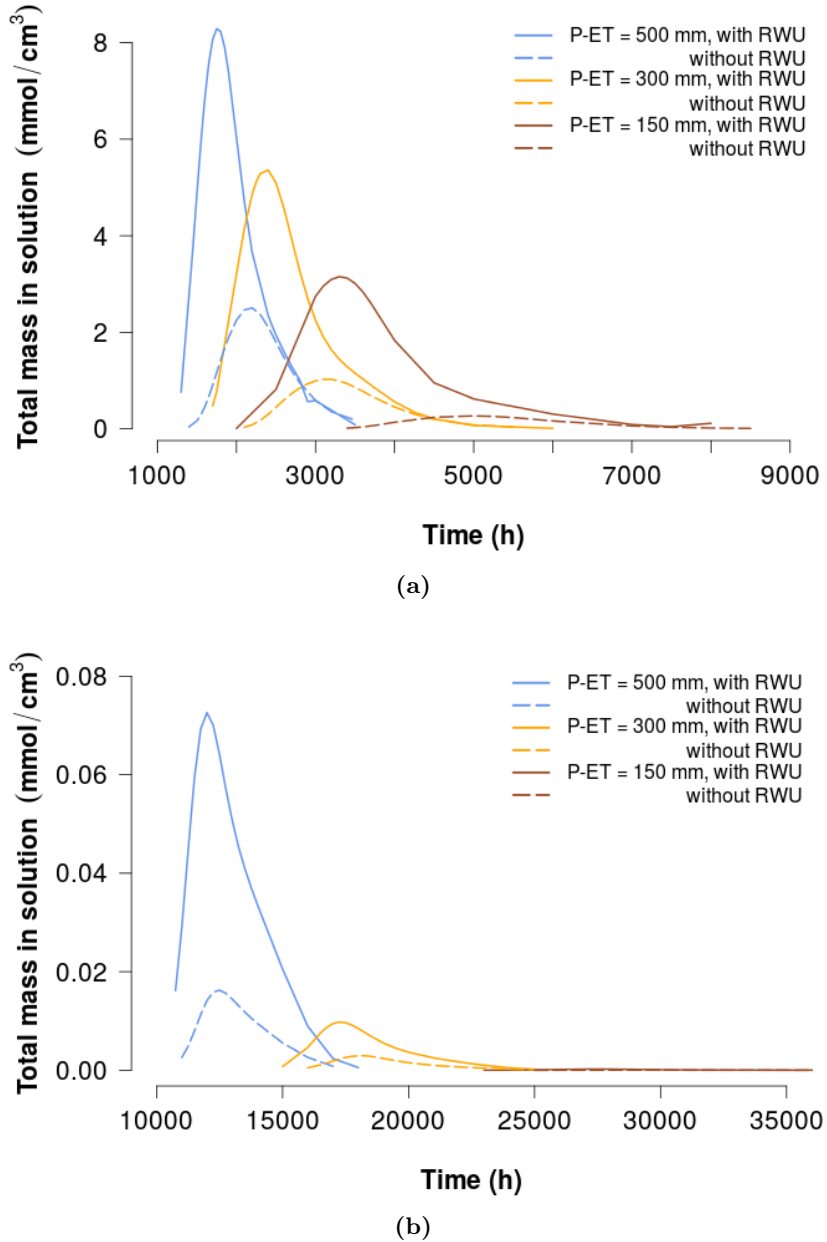


Figure 14: Breakthrough curves of solute over control plane 1 (left) and 2 for the three scenarios with decreasing amount of net infiltration (blue=PET500, yellow=PET300 and red=PET150). Dashed curves show similar simulations with equal net infiltration, but without root water uptake. Degradation constant equal for all simulations. For a more detailed view of the curves in (b), see Figure 22 in Appendix B. For peak values and times, see Table 4

In conclusion, the ratio of leached mass with and without RWU over CP1 and CP2 is largest for the lowest net infiltration. The higher the net infiltration, the smaller becomes the difference on solute leaching of including or not including RWU in the model. Net infiltration is therefore an important variable determining leaching.

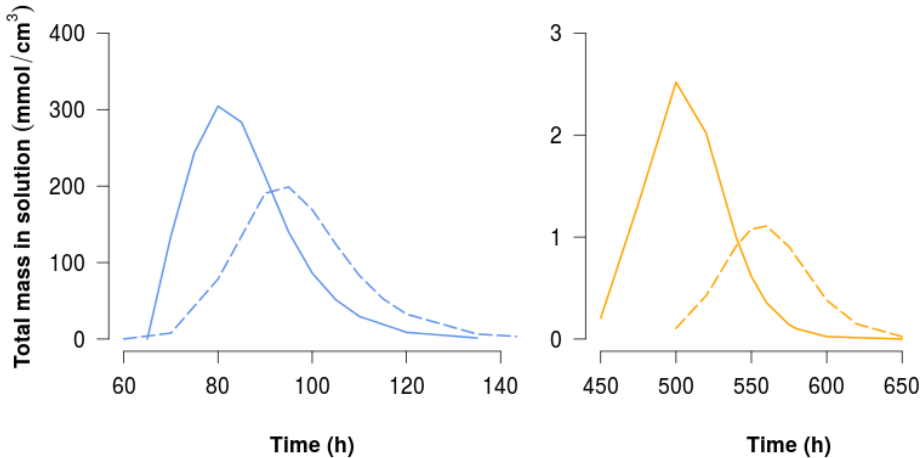


Figure 15: Breakthrough curves of solute over control plane 1 (left) and 2 for a scenario with a critical shift at the root zone with (continuous line) and without (dashed line) root water uptake.

4.6. Solute spreading with critical regime shift at the root zone

As described before, a shift in hydraulic structure can occur when the saturation passes a critical point. To see what this could mean for solute breakthrough in combination with root water uptake, the following scenario was made: a precipitation of 0.4 cm/h is applied to the domain, causing high saturation and a corresponding flow structure. Transpiration by root water uptake amounts to 0.1 cm/h . This reduces the amount of water available for further infiltration to the groundwater to 0.3 cm/h . This flux is lower than the critical flux, and therefore the hydraulic structure will be shifted in this case.

In Figure 15 the breakthrough curves of this situation can be seen. Dashed curves show a similar situation, but without root water uptake, and therefore also without shift in hydraulic structure. The dashed curves have a later breakthrough and are more spread out.

The later breakthrough is a result of the lower initial velocities when the net infiltration is used. In case of RWU, initially the flow velocities are much larger, resulting in a quicker transport. Next to that, it can be seen that the dashed curve is more symmetrical, whereas the continuous curve shows tailing towards the longer travel times.

The difference of the solute breakthrough front because of the shift in preferential flow paths cannot be seen here well, because the spatial differences are evened out. The breakthrough curves show the total solute breakthrough per time step, not the spatial distribution. In Figure 16, however, we see the total mass passing the first control plane at a certain time. The quantities are different because in the simulation without root water uptake the solute has had a longer time to break down. The difference is not as clear as expected. The fact that no shift has taken place in the simulation without root water uptake does not mean a reversed profile is seen. Clearly, this shift in hydraulic structure has taken place above the control plane and the resulting patterns are similar. Therefore, even when saturation and precipitation conditions like these result in a shift in hydraulic structure, the influence on the breakthrough is limited.

In Figure 16 the grey dashed line shows the difference between the two lines by dividing the mass values in a situation with RWU by the mass values of the situation without RWU. The two lines show the mass passing at a certain time step, so no total solute mass. Therefore the tracer front figures, from which this picture is made, should also be considered. In such plots, the front for a situation with RWU has moved slightly further, as expected. The spatial pattern of the

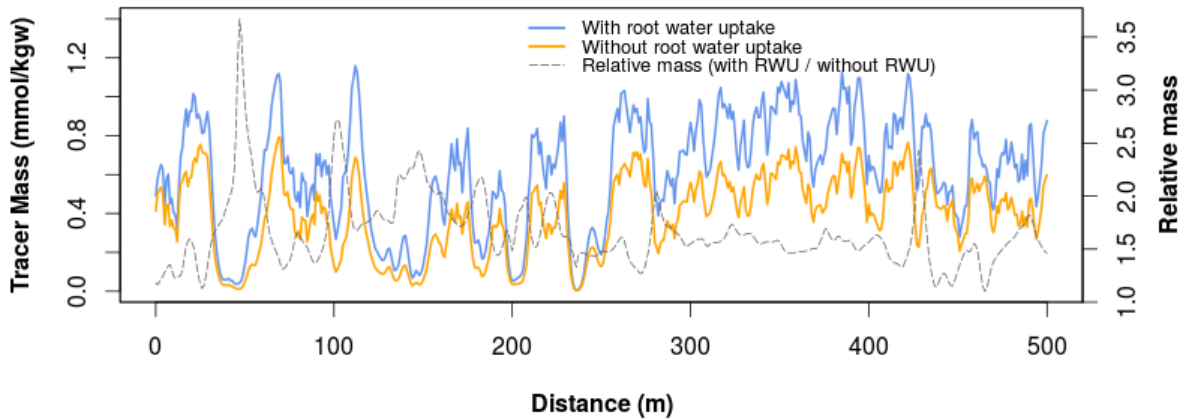


Figure 16: Total mass passing CP1 for similar simulations with (blue) and without RWU, at $t=80$, resp. $t=90h$, where the solute centre of mass is at approximately the same depth.

two fronts is very similar. From Figure 16, it seems that at locations with a high concentration, i.e. locations where the front is about halfway, the difference is limited. However, at locations with lower masses, i.e. locations where the centre of the front has already passed or still has to come, the difference is more substantial. There, the masses are up to three times higher for a case with root water uptake. Apparently, at these places, the difference between the front of which one has moved slightly further is more substantial than around the centre of mass.

The total amount of solute passing the control planes is shown in Table 5. Again, we see here the higher mass passing the control planes for a case with RWU taken into account.

4.7. Influence of the groundwater table depth and root water uptake on solute leaching

Figure 17 shows the breakthrough over control plane 1 in three cases with different groundwater depth. All other conditions are kept the same, i.e. the stochastic field for conductivity and pressure head, the degradation constant and the precipitation and evapotranspiration amounts. The curves are quite similar, but show a certain difference in the height of the peak. As can be seen in Table 5, the total mass that passes CP1 is also similar for the three groundwater depths, slightly higher for a groundwater depth of 2m. This shows that even the conditions further down in the domain can have an influence on the solute above it, although very limited.

We also see an order in the curves: they are ascending, from a slightly higher breakthrough for a shallow groundwater table to a slightly lower breakthrough for a deeper groundwater table. The wetter conditions for the shallow groundwater table could have enhanced the velocities and resulted in an earlier breakthrough with less degradation, explaining the small observed differences. However, calculations show that these differences in saturations are negligible. The leached mass difference for the lowest and highest BTC is about 6%.

This is in accordance with what was found by [25]. They hypothesised that the effect of RWU might become significant in situations where the rooting depth is of the same order of magnitude as the depth to the water table. To analyse different ratios, not the domain size was altered, but the rooting depth. However, in contrast to the hypothesis, there was just a small influence of the variability in rooting depth on the results (spatial covariance of the output variables matric potential ψ and saturation S).

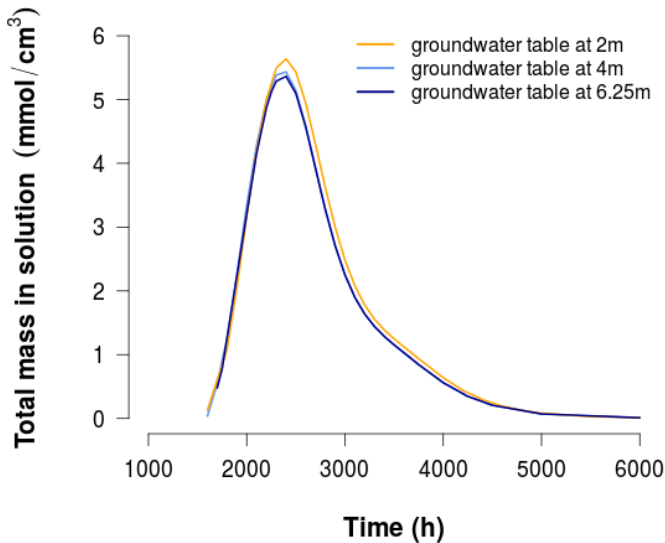


Figure 17: Breakthrough curves of solute over control plane 1 (CP1) for three scenarios with decreasing groundwater depth.

We can conclude that the capillary fringe is thin and that it is not an important influence on saturation and therefore breakthrough in the chosen domain sizes. Depth to the groundwater table is not an important variable when it comes to predicting breakthrough in the upper soil.

4.8. Effect of including root water uptake in a model on solute leaching

When we consider the results from the sections 4.5 and 4.6, we can deduce some more general implications of including root water uptake in solute leaching simulations.

In all shown graphs with breakthrough curves (Figure 14, 15) the dashed curve is clearly different than its continuous counterpart. Quantitatively, differences are shown in Table 5. BTCs show that not including RWU would predict later breakthrough, where root water uptake can significantly enhance breakthrough. Especially in the case where degradation is included, these differences in timing can imply a significantly different amount of solute breaking through. Including root water uptake is therefore important to avoid underestimation of leaching towards the groundwater.

The effect is most strongly visible in cases with low effective infiltration amounts. This becomes clear from Table 6. The ratio of leached solute for a case with RWU over a case without RWU is largest for the lowest net percolation, i.e. the influence of root water uptake on leaching is larger there. The ratio decreases with increasing net infiltration. The difference in travel times is lower there, and therefore also the difference in time for degradation.

Ratios of leaching mass in solution over CP2 shows another pattern: the ratio of solute leaching over CP2 is lower than over CP1 for the lowest-infiltration case ($P - ET = 150\text{mm}$). With increasing net infiltration, the ratio of solute leaching over CP2 becomes larger than the ratio of leached solute over CP1, an ascending pattern. This means that the influence of root water uptake on solute leaching to the groundwater (the whole domain) is becoming relatively larger than the influence of root water uptake on leaching over a plane in the upper zone only.

Apart from that, some differences can be seen in the form of the BTCs. Including root water uptake makes the breakthrough curve more skewed. Tailing of breakthrough curves is a known phenomenon of transport in the unsaturated zone, also in the presence of preferential transport.

E.g. De Smedt (1984) found that this tailing is the result of immobile water, resulting in larger dispersion coefficients than expected on the basis of saturated flow experiments alone [5].

An explanation of the tailing of these curves in a case with root water uptake could be in the difference in relative variance of the conductivity with different wetness. When root water uptake occurs, the top of the domain will be wetter. This brings different conductivity conditions, with different statistics. Variation in the random field that is used in the model, works through in two ways to produce heterogeneity in cases with different wetness. Firstly, there is the variation in K_{sat} following from the soil moisture content via the retention function. Next to that, the fact that we deal with the unsaturated zone means other nonlinear functions do apply, and the hydraulic conductivity therefore has added variation.

To test if this is indeed the case, the coefficient of variation (CV) has been calculated. The fields for situations with different wetness can then be compared. This has been done for the simulations of the basic situation, Rw_{basic} , and for the situation in which a shift occurs. The CV has been calculated for the fields of K and $\ln K$, for the whole domain and for the part of the domain above CP1. However, as can be seen in Table 7, no clear differences show up. The tailing in the breakthrough curves can therefore not be explained by the added variation in conductivity in wetter situations.

Table 7: Coefficient of variation for conductivity fields.

	K Whole domain	K Domain above CP1	$\ln K$ Whole domain	$\ln K$ Domain above CP1
RWU Basis	5.74	0.723	-0.487	-0.343
RWU Basis, no RWU	5.76	0.731	-0.484	-0.317
RWU Shift	0.773	0.413	1.034	1.10
RWU Shift, no RWU	0.816	0.392	1.13	1.23

Russo (1998), described in a 3D numerical analysis, how a velocity fluctuation field is formed by spatially variable soil hydraulic properties with variable climatic conditions and root water uptake. He describes how these velocity fluctuations act to spread the solute sideways, thereby smoothing out extremes, while longitudinal spreading is decreased. This has been explained by root water uptake, which produced lower conductivities, thus lower solute velocity and therefore vertical compression. The heterogeneity is smoothed. Consequently, the solute moves down slower and the concentration profile is less skewed. Foussereau (2000) also describes the influence of the moisture content on the form of the breakthrough curve. A finer textured soil with higher residual water contents exhibited delayed travel times and increased spreading.

We indeed see that less vertical spreading occurs in a case with root water uptake, as the breakthrough curves are more peaked. However, this is not a result of the drier soil, like Russo stated, as we take into account that the net infiltration is the same in cases with and without root water uptake. The soil is even wetter in the upper part of the domain where the roots have not taken up the excess of water yet. Also, solute movement is not slower, but quicker than in a case without root water uptake.

All in all, root water uptake is not to be ignored when predicting solute breakthrough well is the aim, as leaving it out would underestimate timing and amount of leaching. Especially for the low-infiltration cases this is important, as the travel times are largest here and therefore the differences are larger as well. Another reason to include RWU in a model is because its influence on the form of the breakthrough curve.

5. Conclusion

In this report, the results are shown of simulations of solute transport in a heterogeneous unsaturated medium. Steady-state and transient simulations of the spreading of a conservative chemical are performed, where soil heterogeneity in the domain is simulated using an autocorrelated field of the scaling parameter. Several simulations with varying inflow, timing of solute application and use of root water uptake are formulated to study flow and transport.

The main findings can be summarised as follows:

1. Simulations show more connected and pronounced preferential flow paths in case of a low inflow in comparison to a case with high inflow. The correlation lengths of the concentration fields are indeed larger in this case. This could have to do with the distance of the low flow from the critical point in saturation which determines the connectedness of the hydraulic structure. However, as just two situations are simulated, extrapolations cannot be made to know how the hydraulic structure changes in intermediate or more extreme high or low flow cases. Furthermore, correlation lengths are mostly smaller than the input scaling parameter used to simulate heterogeneity in hydraulic conductivity and pressure heads, indicating additional heterogeneity.
2. In the transient simulations the shift of flow paths can be seen, as has been found before for two steady state situations [22]. This shift has been considered in simulations with solute movement. When a high flux overtakes a low one, the water and solute that came first with the low infiltration are moved with the passing high-flux water, into the high-conductivity flow paths.
3. Another feature that is shown by the output of the simulations is the influence of initial conditions: low flow initial conditions make that the solute front lags behind slightly on the front in comparison to a situation where it would have been infiltrated with high flow initial conditions. When this is applied to a realistic situation, we can think of e.g. rain/irrigation events. When the soil is dry before irrigation contaminants will move down slower than in a situation in which the soil was wetter just before the rainfall.
4. For a case where a low flux is followed by a high one, we see that the solute which is applied with the high flux overtakes the first solute, applied with a low flux. During the overtaking process, the low-flux front is compressed. This becomes important when the considered solute is a degrading chemical. Processes increasing the residence time in the unsaturated zone will then imply that more degradation can take place and less leaching to the groundwater occurs. However, when a front of higher flow passes chemicals which were captured in flow paths of low flow, it will transport these down. Then chemicals are transported down more quickly.
5. From the simulations it also becomes clear that the solute front lags behind on the moisture front when high flow follows low flow. The effect is important in assessing water quality of aquifers and making groundwater recharge estimations. For the first, assessing groundwater vulnerability, using contaminant travel times over the unsaturated zone is required, whereas estimates of recharge changes are best made using the pressure-based velocity. Estimation based on the infiltration-front velocity would overestimate the leaching.
6. Including root water uptake is certainly important to predict solute leaching well. The higher velocities in the root zone, compared to a case where only the net percolation

is applied, cause the solute to spread differently, thereby influencing the form of the breakthrough curve. The solute breaks through earlier, with higher peaks (due to less time for degradation) and in a skewed way.

7. Furthermore, a set of conditions have been altered to see their influence on breakthrough. Decreasing the net percolation makes the previously formulated effects become stronger, i.e. not including root water uptake meant an even larger difference in peak timing, maximum and symmetry. The depth to the groundwater table was also considered. It could be concluded that in this case, the capillary fringe was not influencing saturation conditions enough to change breakthrough over the first control plane. Also, for the considered parametrisation, even when saturation and precipitation conditions result in a shift in hydraulic structure, the influence on the breakthrough is limited.

In conclusion, we see that root water uptake should not be ignored when solute leaching is considered. Ignoring this process would imply an overestimation of breakthrough time and underestimation of breakthrough mass. However, as root water uptake is a complicated process to model, it is often left out and a simplification is assumed. Therefore, it would be good to use the results of the RWU-scenarios to find a reverse method to include the realistic effects of root water uptake in a simpler model without having to take into account the detailed processes. This can be done by calculating the effective velocity q through the root zone for a case with RWU. Then in a similar model without RWU, the precipitation can be increased by this amount (= half the water that the root zone would take up for transpiration). Then, BTCs over the first control plane can be compared for the case including RWU and the case with increased inflow. They are aimed for to become similar. Root water uptake is then mimicked by taking a substitute term for the higher velocities normally taking place in a case with root water uptake.

In this model many simplifications have been made. Just one realisation of the stochastic distribution has been used. Also, in reality, the solute is not behaving ideally, but subject to more complex degradation, retardation and interacting with the matrix in other ways. Furthermore, the used temporal patterns are strongly simplified. Despite these limitations, the processes found here are important to consider when studying chemical transport in an heterogeneous unsaturated zone, as they could either mean increased leaching to the groundwater or increased residence time in the unsaturated zone.

It would be interesting to include more processes in this model to get results that are more applicable to reality. Degradation of the Monod-type could be incorporated into this model. When the solute moves into a different flow path at a regime shift, the solute could encounter an environment which enhances or decreases degradation. Next to that, a realistic precipitation time series could be used as input.

6. Acknowledgements

I would like to thank my supervisors Sjoerd van der Zee and Toon Leijnse for their help and guidance in this project! Also thanks to Annette Dathe, Helen French and Perrine Fernandez for the interesting and fun days in Ås, Márcia Batalha for her help with my questions about the modelling, and my fellow students and friends for their advice on my report.

References

- [1] BIRKHOLZER, J., AND TSANG, C. Solute channeling in unsaturated heterogeneous porous media. *Water Resources Research* 33, 10 (1997), 2221–2238.
- [2] BIRÓ, B., TOSCANO, G., HORVÁTH, N., MATICS, H., DOMONKOS, M., SCOTTI, R., RAO, M., WEJDEN, B., AND FRENCH, H. K. Vertical and horizontal distributions of microbial abundances and enzymatic activities in propylene-glycol-affected soils. *Environmental Science and Pollution Research* 21, 15 (2014), 9095–9108.
- [3] BUTTERS, G. L., AND JURY, W. A. Field scale transport of bromide in an unsaturated soil: 2. dispersion modeling. *Water Resources Research* 25, 7 (1989), 1583–1589.
- [4] CLOTHIER, B. E., AND GREEN, S. R. Rootzone processes and the efficient use of irrigation water. *Agricultural Water Management* 25, 1 (1994), 1 – 12.
- [5] DE SMEDT, F., AND WIERENGA, P. J. Solute transfer through columns of glass beads. *Water Resources Research* 20, 2 (1984), 225–232.
- [6] EUROPEAN PARLIAMENT, COUNCIL OF THE EUROPEAN UNION. Directive 2006/118/ec of the european parliament and of the council on the protection of groundwater against pollution and deterioration. *Official Journal of the European Union* (2006).
- [7] FLURY, M., FLÜHLER, H., JURY, W. A., AND LEUENBERGER, J. Susceptibility of soils to preferential flow of water: A field study. *Water Resources Research* 30, 7 (1994), 1945–1954.
- [8] FOOD AND AGRICULTURE ORGANISATION - WATER DEVELOPMENT AND MANAGEMENT UNIT. Crop water information for wheat, 2015.
- [9] FRENCH, H., DER ZEE, S. V., AND LEIJNSE, A. Transport and degradation of propylene-glycol and potassium acetate in the unsaturated zone. *Journal of Contaminant Hydrology* 49, 1–2 (2001), 23 – 48.
- [10] FRENCH, H. K., VAN DER ZEE, S. E. A. T. M., AND LEIJNSE, A. Differences in gravity-dominated unsaturated flow during autumn rains and snowmelt. *Hydrological Processes* 13, 17 (1999), 2783–2800.
- [11] GLASS, R. J., STEENHUIS, T. S., AND PARLANGE, J.-Y. Mechanism for finger persistence in homogeneous, unsaturated, porous media: theory and verification. *Soil Science* 148, 1 (1989), 60–70.
- [12] HELLSTÉN, P., AND NYSTÉN, T. Migration of alternative de-icers in unsaturated zone of aquifers - in vitro study. *Water Science & Technology* 48, 9 (2003), 45–50.

- [13] KUNTZ, D., AND GRATWOHL, P. Comparison of steady-state and transient flow conditions on reactive transport of contaminants in the vadose soil zone. *Journal of Hydrology*, 369 (2009), 225–233.
- [14] LEIJNSE, A. *PPHP2V2 documentation*, 2015.
- [15] LISSNER, H., WEHRER, M., JARTUN, M., AND TOTSCHE, K. Degradation of deicing chemicals affects the natural redox system in airfield soils. *Environmental Science and Pollution Research* 21, 15 (2014), 9036–9053.
- [16] LIU, Y., STEENHUIS, T. S., AND PARLANGE, J.-Y. Formation and persistence of fingered flow fields in coarse grained soils under different moisture contents. *Journal of Hydrology* 159, 1 (1994), 187 – 195.
- [17] MILLER, E. E., AND MILLER, R. D. Physical theory for capillary flow phenomena. *Journal of Applied Physics* 27, 4 (1956).
- [18] NIMMO, J. R. Vadose water. *Encyclopedia of Inland Waters* 1 (2009), 766–777.
- [19] PYRCZ, M. J., AND DEUTSCH, C. V. The whole story on the hole effect. *Centre for Computational Geostatistics, University of Alberta, Edmonton* (2003).
- [20] RAATS, P. *Tracing parcels of water and solutes in unsaturated zones*. Pollutants in Porous Media: The Unsaturated Zone between Soil Surface and Groundwater, 1984.
- [21] RASMUSSEN, T. C., BALDWIN, R. H., DOWD, J. F., AND WILLIAMS, A. G. Tracer vs. pressure wave velocities through unsaturated saprolite.
- [22] ROTH, K. Steady state flow in an unsaturated, two-dimensional, macroscopically homogeneous, miller-similar medium. *Water Resources Research* 31, 9 (1995), 2127–2140.
- [23] ROTH, K., AND HAMMEL, K. Transport of conservative chemical through an unsaturated two-dimensional miller-similar medium with steady state flow. *Water Resources Research* 32, 6 (1996), 1653–1663.
- [24] ROYAL NETHERLANDS METEOROLOGICAL INSTITUTE (KNMI). Overzicht van de neerslag en verdamping in nederland, 2015.
- [25] RUBIN, Y., AND OR, D. Stochastic modeling of unsaturated flow in heterogeneous soils with water uptake by plant roots: The parallel columns model. *Water Resources Research* 29, 3 (1993), 619–631.
- [26] RUSSO, D., ZAIDEL, J., AND LAUFER, A. Stochastic analysis of solute transport in partially saturated heterogeneous soil: 2. prediction of solute spreading and breakthrough. *Water Resources Research* 30, 3 (1994), 781–790.
- [27] SCHOENBERG, T., VELTMAN, S., AND SWITZENBAUM, M. Kinetics of anaerobic degradation of glycol-based type i aircraft deicing fluids. *Biodegradation* 12, 1 (2001), 59–67.
- [28] SCHOTANUS, D., MEEUSSEN, J., LISSNER, H., VAN DER PLOEG, M., WEHRER, M., TOTSCHE, K., AND VAN DER ZEE, S. Transport and degradation of propylene glycol in the vadose zone: model development and sensitivity analysis. *Environmental Science and Pollution Research* 21, 15 (2014), 9054–9066.

[29] SCHOTANUS, D., VAN DER PLOEG, M. J., AND VAN DER ZEE, S. E. A. T. M. Quantifying heterogeneous transport of a tracer and a degradable contaminant in the field, with snowmelt and irrigation. *Hydrology and Earth System Sciences* 16, 8 (2012), 2871–2882.

[30] STEENHUIS, TAMMO S. AND MUCK, R. E. Preferred movement of nonad- sorbed chemicals on wet, shallow, sloping soils. *Journal of Environmental Quality* 17, 3 (1988).

[31] TOSCANO, G., COLARIETI, M., ANTON, A., GRECO, G., AND BIRÓ, B. Natural and enhanced biodegradation of propylene glycol in airport soil. *Environmental Science and Pollution Research* 21, 15 (2014), 9028–9035.

[32] VAN DAM, J., DE ROOIJ, G., HEINEN, M., AND STAGNITTI, F. Concepts and dimensionality in modeling unsaturated water flow and solute transport. *Frontis* 6 (2005), 1–36.

[33] VAN GENUCHTEN, M. T. A closed-form equation for predicting the hydraulic conductivity of unsaturated soils. *Soil Science Society of America Journal* 44, 5 (1980), 892–898.

[34] VANDERBORGH, JANAND KASTEEL, R. V. H. Stochastic continuum transport equations for field-scale solute transport. *Vadose Zone Journal* 5, 1 (2006), 184–203.

[35] VELTMAN, S., SCHOENBERG, T., AND SWITZENBAUM, M. Alcohol and acid formation during the anaerobic decomposition of propylene glycol under methanogenic conditions. *Biodegradation* 9, 2 (1998), 113–118.

[36] VOGEL, T. Swmii - numerical model of two-dimensional flow in a variably saturated porous medium. *Research Rep. No. 87 Wageningen Agricultural University, Department of Hydraulics and Catchment Hydrology* (1987).

[37] VOGEL, T., CISLEROVA, M., AND HOPMANS, J. W. Porous media with linearly variable hydraulic properties. *Water Resources Research* 27, 10 (1991), 2735–2741.

[38] VRUGT, J. A.; HOPMANS, J. W. v. J. Calibration of a two-dimensional root water uptake model. *Soil Science Society of America Journal* 65, 4 (2001).

[39] WARRICK, A. W., BIGGAR, J. W., AND NIELSEN, D. R. Simultaneous solute and water transfer for an unsaturated soil. *Water Resources Research* 7, 5 (1971), 1216–1225.

[40] WEJDEN, B., AND ØVSTEDAL, J. *Contamination and degradation of de-icing chemicals in the unsaturated and saturated zones at Oslo airport, Gardermoen, Norway*, vol. 74 of *NATO Science Series*. Springer Netherlands, 2006.

[41] WHITE, R. E., DYSON, J. S., GERSTI, Z., AND YARON, B. Leaching of herbicides through undisturbed cores of a structured clay soil. *Soil Science Society of America* 50, 2 (1986).

[42] WU, J., ZHANG, R., AND GUI, S. Modeling soil water movement with water uptake by roots. *Plant and Soil* 215, 1 (1999), 7–17.

[43] ŠIMŮNEK, J., JARVIS, N. J., VAN GENUCHTEN, M., AND GÄRDENÄS, A. Review and comparison of models for describing non-equilibrium and preferential flow and transport in the vadose zone. *Journal of Hydrology* 272, 1–4 (2003), 14 – 35. Soil Hydrological Properties and Processes and their Variability in Space and Time.

- [44] ŠIMŮNEK, J., VAN GENUCHTEN, M. T., AND ŠEJNA, M. Development and applications of the hydrus and stanmod software packages and related codes. *Vadose Zone Journal* 7, 2 (2008), 587–600.
- [45] ŠIMŮNEK, J., AND ŠEJNA, M. *HYDRUS Technical Manual*, 2 ed. PC-Progress, 2011.

Appendices

A. Model runs

Table 8: Print times for each run (in hours). $L=$ low flow, $H=$ high flow. 1 of 2 at the end of the code indicates the amount of tracers added. Bold number: solute added at this timestep.

L	H	L1	H1	LH1	HL1	LH2	HL2
1	1	1	1	1	1	1	1
1500	25	1500	25	1500	25	1500	25
3000	50	3000	50	3000	50	3000	50
4500	75	4500	75	4500	75	4500	75
6000	100	6000	100	6000	100	6000	100
7500	1100	7500	1100	7500	125	6015	125
10000	2200	10000	2200	8500	150	6030	150
15000	3200	15000	3200	8515	200	6045	200
20000	4200	20000	3225	8530	250	6060	250
24000		22000	3250	8545	300	6075	300
		24000	3275	8560	350	6090	350
		26000	3300	8575	400	6105	400
		28000	3325	8590		6120	600
		30000	3350	8605		6135	800
		32000	3375	8620		6150	1000
		34000	3400	8635			2000
		36000					4000
		38000					6000
							10000
							14000

Table 9: Variable boundary conditions for the different runs: time, precipitation and concentration are given

H1				L1			
<i>Time</i> <i>h</i>	<i>Precipitation</i> <i>cm/h</i>	<i>Solute 1</i> <i>mmol/cm³</i>	<i>Solute 2</i> <i>mmol/cm³</i>	<i>Time</i> <i>h</i>	<i>Precipitation</i> <i>cm/h</i>	<i>Solute 1</i> <i>mmol/cm³</i>	<i>Solute 2</i> <i>mmol/cm³</i>
1	1.138			1	3.6E-3		
3199	1.138			19999	3.6E-3		
3200	1.138	1.7575		20000	3.6E-3	555.5	
3400	1.138			38000	3.6E-3		
HL1_{begin}				LH1_{begin}			
1	1.138	1.7575		1	3.6E-3	555.5	
74	1.138			8499	3.6E-3		
75	3.6E-3			8500	1.13 8		
400	3.6E-3			8635	1.13 8		
HL1_{shift}				LH1_{shift}			
1	1.138			1	3.6E-3		
100	1.138			8499	3.6E-3		
101	3.6E-3	555.5		8500	1.13 8	1.7575	
400	3.6E-3			8635	1.13 8		
HL2				LH2			
1	1.138	1.7575		1	3.6E-3	555.5	
100	1.138			8499	3.6E-3		
101	3.6E-3		555.5	8500	1.138		1.7575
14000	3.6E-3			8635	1.138		

Table 10: Detailed description of all RWU simulations

Run name	Description	P (mm/y)	ET (mm/y)	Deg. rate (/h)
RWU ₂	Groundwater at 2 m depth	850	550	-3.5×10^{-4}
RWU ₄	Groundwater at 4 m depth	850	550	-3.5×10^{-4}
RWU PET300	Groundwater at 6.25 m depth	850	550	-3.5×10^{-4}
RWU PET300 _N	Without RWU, same net infiltration	300	-	-3.5×10^{-4}
RWU PET150	Net infiltration 150 mm/y	700	550	-3.5×10^{-4}
RWU PET150 _N	Net infiltration 150 mm/y, no RWU	150	-	-3.5×10^{-4}
RWU PET500	Net infiltration 500 mm/y	1050	550	-3.5×10^{-4}
RWU PET500 _N	Net infiltration 150 mm/y, no RWU	500	-	-3.5×10^{-4}
RWU Shift	With shift in hydraulic structure	0.4 cm/h	0.1 cm/h	-9.21×10^{-3}
RWU Shift _N	Same net infiltration, no RWU and no shift	0.3 cm/h	-	-9.21×10^{-3}

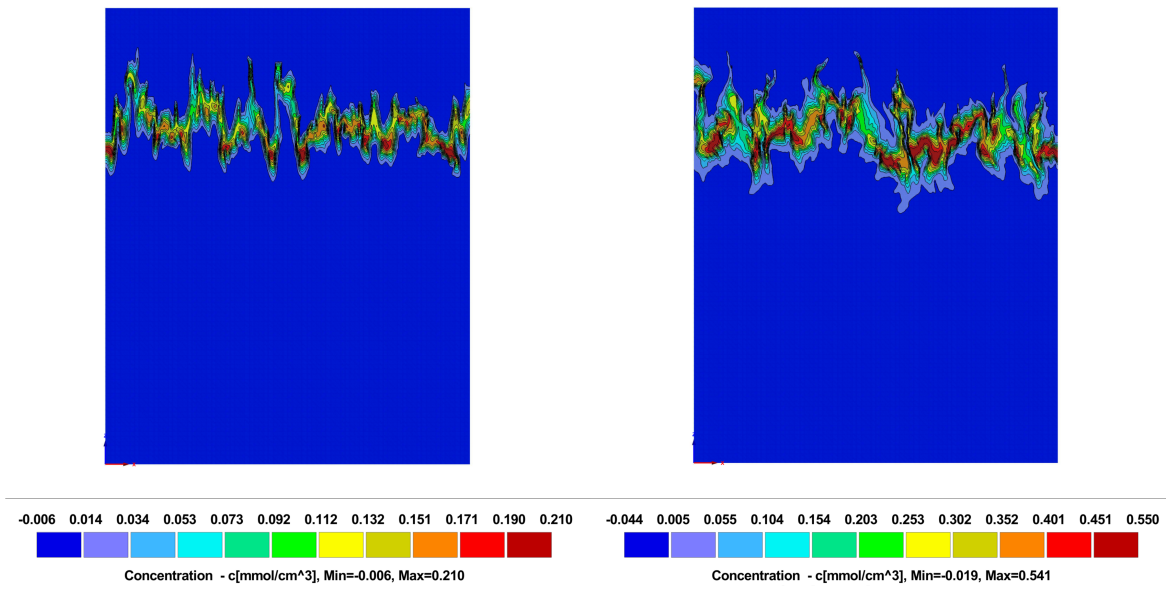
B. Figures

Figure 18: Output concentration fields for H1 (left, at $t=3250h$) and L1 (for $t=26000h$).

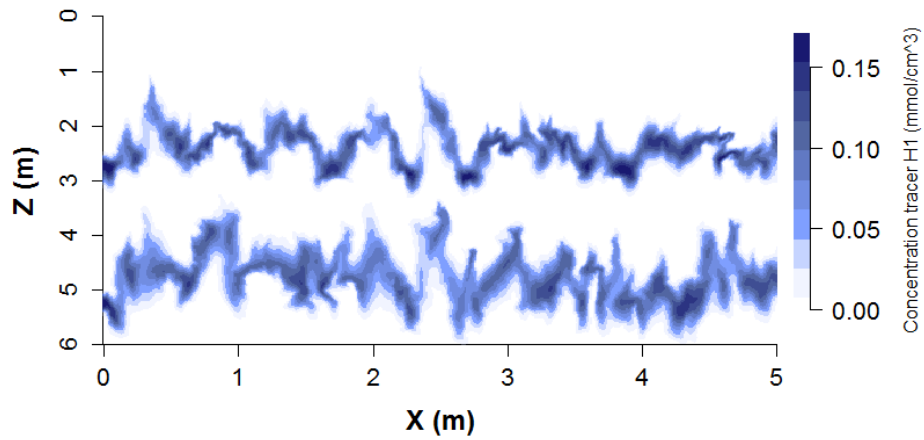


Figure 19: Solute fronts for the run H1, at $t=3275$ and $t=3350h$. This figure is used to find the concentration differences shown in Figure 8.

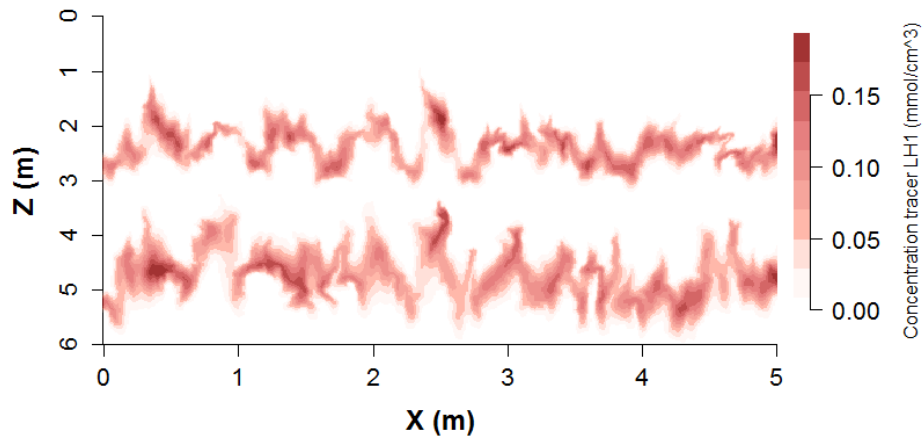


Figure 20: Solute fronts for the run LH1, at $t=6075$ and $t=6150h$. This figure is used to find the concentration differences shown in Figure 8.

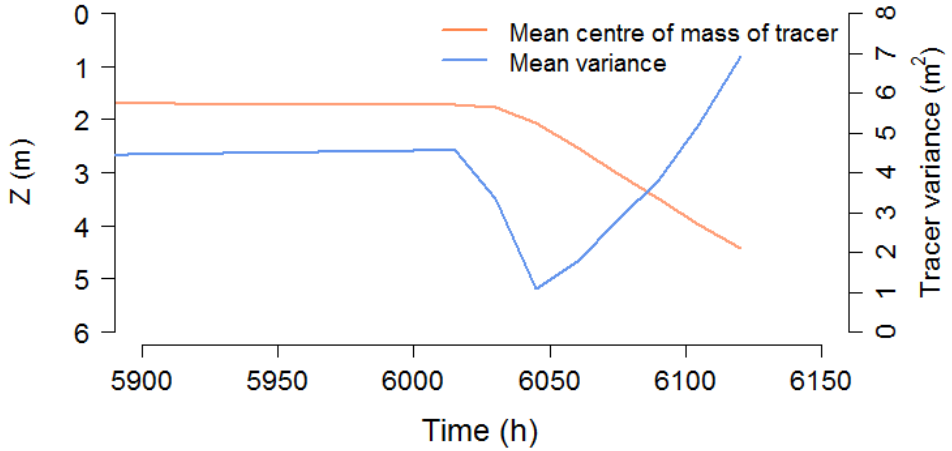


Figure 21: Depth of the centre of mass of the tracer and its variance for the case LH2, tracer 1. Shift to high flux at $t=6000\text{h}$. For complete Figure see 12b.

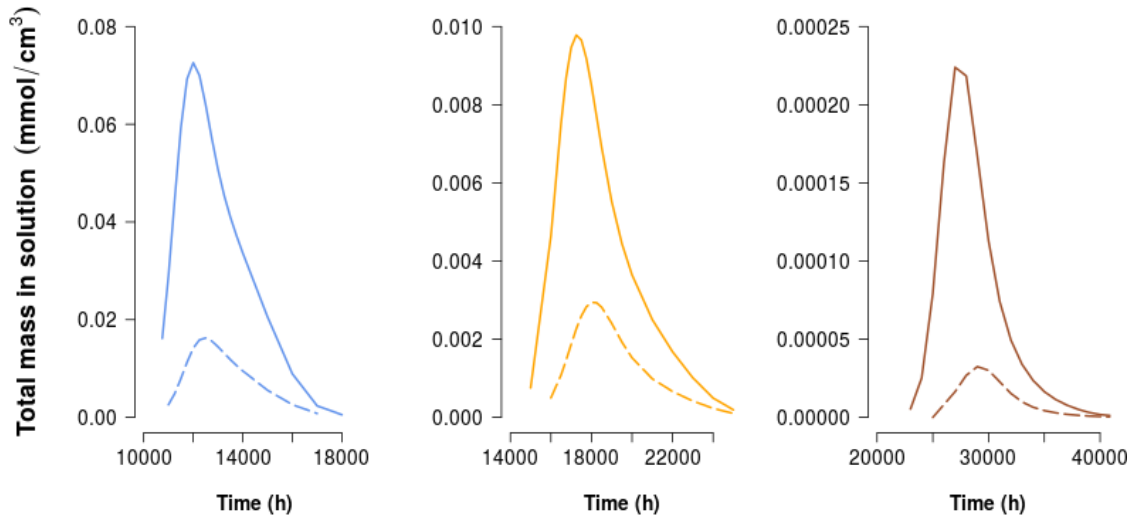


Figure 22: As in Figure 14b, breakthrough curves of solute over control plane 2 (CP2). Now for the three scenario's separately. Blue=PET500, Yellow=PET300 and Red=PET150. Dashed curves show similar runs with equal net infiltration, but without root water uptake. Degradation constant equal for all runs.